

This is a preprint of a peer-reviewed article accepted at the journal CLIMATE DYNAMICS, with the DOI 10.1007/s00382-023-06857-w. The manuscript posted here is a preprint submitted to EarthArXiv.

Continental configuration controls the base-state water vapor greenhouse effect: lessons from half-land, half-water planets

Marysa M. Laguë^{1,2*}, Gregory R. Quetin³, Sarah Ragen⁴
and William R. Boos^{5,6}

¹Coldwater Lab, Center for Hydrology, University of Saskatchewan, 1151 Sidney Street, Unit 116, Canmore, T1W 3G1, Alberta, Canada.

^{2*}Department of Atmospheric Sciences, University of Utah, 135 S 1460 E, ROOM 819, Salt Lake City, 84112-0102, UT, USA
<https://orcid.org/0000-0001-8513-542X>.

³Department of Geography, University of California, Santa Barbara, 1832 Ellison Hall, Santa Barbara, 93106-4060, CA, USA
<https://orcid.org/0000-0002-7884-5332>.

⁴School of Oceanography, University of Washington, 1501 NE Boat St, Seattle, 98195, Washington, USA
<https://orcid.org/0000-0003-0987-6060>.

⁵Department of Earth and Planetary Science, University of California, Berkeley, 307 McCone Hall, Berkeley, 94720-4767, California, USA.

⁶Climate and Ecosystem Sciences Division, Lawrence Berkeley National Lab, 1 Cyclotron Rd, Berkeley, 94720, California, USA
<https://orcid.org/0000-0001-9076-3551>.

*Corresponding author(s). E-mail(s): marysa.lague@utah.edu;

Abstract

The distribution of land and ocean on Earth's surface shapes the global atmospheric circulation and climate by modulating fluxes of water and energy between the surface and the atmosphere. Here we rearranged land in an idealized climate model to explore the effect

of eight simplified continental configurations on global climate, finding several counterintuitive results. The limited capacity of land to hold water and the smaller heat capacity of land compared to ocean—rather than surface albedo differences—are the primary drivers of continental control on global mean temperature. Specifically, the presence of land in certain locations can enhance tropospheric water vapor content, increasing the greenhouse effect and clear-sky shortwave absorption; these effects can warm the planet more than the cooling effect of higher land surface albedos. For example, continental configurations with land in polar regions and large tropical oceans have the warmest, wettest global climates. Configurations with large tropical land masses are not hot desert planets, but have the coolest global climates due to reduced evaporation and thus reduced atmospheric water vapor compared to configurations without land in the tropics. Interactions between the small heat capacity of land and the seasonal cycle can lead to certain continental configurations having even warmer, wetter atmospheres than an aquaplanet. Our results demonstrate that different configurations of land, such as those obtained through past tectonic movement or on rocky exoplanets, set planetary climate through mechanisms beyond those involving surface albedo or orographic effects.

Keywords: Water Vapor, Climate, Continents, Land-atmosphere Interactions

1 Introduction

The distribution of continents on Earth’s surface alters both terrestrial and global climate in myriad ways: by modulating surface-atmosphere exchange of water and energy, shaping atmospheric circulation patterns, and delineating ocean basins. Despite its importance, the fundamental role of continental distribution in setting Earth’s base-state climate remains poorly understood. In this study, we explore how the distribution of land on Earth’s surface alters global evaporation patterns and water vapor concentrations, with implications for global mean surface temperatures and climate.

Physical differences between the land and the oceans alter the way the overlying atmosphere interacts with either surface. The land tends to be brighter, drier, rougher, and have a lower heat capacity than the ocean (Budyko, 1961, 1969; Payne, 1972; Bonan, 2008; Jin et al, 2004; Wiscombe and Warren, 1980; Sud et al, 1988; Cess and Goldenberg, 1981; North et al, 1983). Oceans can redistribute energy in the climate system by moving heat laterally while the land cannot (Loft, 1918; Richardson, 1980; Ferrari and Ferreira, 2011). Additionally, while water for evaporation is effectively unlimited in the oceans, the availability of water for evaporation to the atmosphere varies widely over different land regions as a function of the local climate (Baldocchi et al, 1997). Terrestrial evaporation and the surface supply of water varies seasonally and behaves differently under different climates. Moreover, while the evaporation

from the ocean is governed by atmospheric inputs (i.e. wind speed and radiation), the evaporation from the land surface also varies with soil moisture and physical properties of soil and vegetation that provide resistance to terrestrial evaporation (Manabe, 1969; Bonan, 2008).

In slab ocean aquaplanet simulations, the organization of tropical rainfall, the location of the extratropical jet, and the strength of the Hadley circulation are all shown to be impacted by changes in atmospheric water vapor, sea surface temperature, and solar insolation (Kirtman and Shukla, 2000; Barsugli et al, 2005; Kang et al, 2008, 2009; Voigt et al, 2014). The influence of continental configuration on atmospheric water vapor remains largely unexplored; however, recent work has shown that changes in terrestrial evaporation can drastically alter global-scale climate by modifying the total amount of atmospheric water vapor, a strong greenhouse gas (Laguë et al, 2021). In addition, other aquaplanet studies with dynamical oceans illuminate the connection between the distribution of meridional boundaries in the ocean and meridional heat transport, demonstrating how different climates can develop as a result of continental distribution (Enderton and Marshall, 2009; Ferreira et al, 2010).

In the modern continental configuration, changes in land surface properties generate large changes in both surface climate and global-scale circulation (Shukla and Mintz, 1982; Charney et al, 1975; Davin et al, 2010; Laguë et al, 2019). Moreover, the complex orography of mountain ranges impacts atmospheric circulation and generates large climate impacts over both land and ocean regions (Queney, 1948; Eliassen and Palm, 1960; Manabe and Terpstra, 1974; Held, 1985; McFarlane, 1987; Held et al, 2002; Maroon et al, 2015; White et al, 2017). While this study focuses on the impact of continental distribution on temperatures, the impact of the location and size of continents on rainfall has been explored extensively in monsoon literature (Dirmeyer, 1998; Yasunari et al, 2006; Maroon and Frierson, 2016; Zhou and Xie, 2018; Hui and Bordoni, 2021). Continental extent also modulates the response of precipitation to reduced terrestrial evaporation (Pietschnig et al, 2021).

Idealized modelling studies have further explored how the distribution of land impacts temperature by allowing for albedo feedbacks (Barron et al, 1984) as well as by altering the rate of CO₂ weathering and thus the strength of the CO₂ greenhouse effect (Worsley and Kidder, 1991). Latitudinal variations in albedo are driven directly by land distribution and indirectly through impacts on clouds and sea-ice (Enderton and Marshall, 2009; Voigt et al, 2014). The temperature at each latitude is largely modulated by the meridional heat transport (Pierrehumbert, 2010). Previous theory argues that heat transports by both the atmosphere and ocean, in turn, are largely insensitive to details of the dynamics responsible for the transport of heat, but rather depend more strongly on the mean planetary albedo and the equator to pole albedo gradient (Stone, 1978; Enderton and Marshall, 2009) as well as the evaporation and condensation of water (Fajber and Kushner, 2021).

093
094
095
096
097
098
099
100
101
102
103
104
105
106
107
108
109
110
111
112
113
114
115
116
117
118
119
120
121
122
123
124
125
126
127
128
129
130
131
132
133
134
135
136
137
138

139 The role of land distribution in modulating global climate has implications
140 for improving our understanding of climate in Earth’s geologic past. Recon-
141 structions of Earth’s continental configuration over the last several hundred
142 million years span a wide range of continental distributions, sometimes with
143 land clustered into supercontinents, sometimes with land spread widely across
144 the globe as in the modern era (Merdith et al, 2021). Simulations of paleocli-
145 mate include continental configurations vastly different to that of the modern
146 world to study the transition between glacial and interglacial periods (Hoff-
147 man and Schrag, 2002; Hoffman et al, 2017; Voigt et al, 2012), mass extinction
148 events (Penn et al, 2018), and climatic changes due to the opening and closing
149 of oceanic gateways (Straume et al, 2020).

150 We also expect to see different land arrangements on other planets. The
151 habitability of exoplanets is a topic of interest to the astrobiology community
152 (Méndez et al, 2021). The search for planets in the habitable zone hinges on
153 locating the distance from a star that would allow for the presence of liquid
154 water on a planet (a liquid environment is an expected requirement for life
155 and water is the most abundant, common liquid in the universe) (Baross et al,
156 2007). While it is common to find exoplanets within the habitable zone of a star
157 (Burke et al, 2015), whether or not those planets are actually habitable is dif-
158 ficult to determine (Kite and Ford, 2018). Planets with a vast range of masses,
159 sizes, and orbits have been detected (Seager, 2013), with an anticipated wide
160 range of variability in atmospheric mass and composition; the surface proper-
161 ties of those planets further modulate the planet’s habitability (Rushby et al,
162 2020). The presence of liquid water is often used to determine the habitabil-
163 ity of a planet (Seager, 2013); however, the distribution of hospitable surface
164 climates across a planet will depend on local surface climate.

165 In this study, we explore and compare the climates of eight Earth-like
166 planets, which differ only in their continental configuration. Land differs from
167 ocean in the simulations presented here in three key ways: it has a higher
168 albedo; it has a smaller heat capacity; and it has a limited capacity to hold
169 and evaporate water, with increased resistance to evaporation when the land is
170 not saturated. These differences alter the fluxes of water and energy between
171 the surface and the atmosphere over land vs. ocean, leading to changes in both
172 local surface climate and global-scale climate.

173 We show that the distribution of continents exerts a fundamental control
174 on global climate, even in a model without full representation of the differences
175 between land and ocean. We investigate how the distribution of land and
176 ocean alter planetary surface albedo, total absorbed shortwave radiation at
177 the surface, atmospheric water vapor and the water vapor greenhouse effect,
178 and atmospheric feedbacks resulting from differences in land vs. ocean heat
179 capacity. We conclude with a discussion of the role of land in modulating the
180 base-state climate of a planet, as well as the sensitivity of that climate to
181 changes in terrestrial evaporation.

182

183

184

2 Methods

2.1 Model

In this study, we use Isca (Vallis et al, 2018), an idealized global circulation model (GCM) to explore the climate of an Earth-like planet with various idealized continental configurations. There is a seasonal cycle in insolation (23.439° obliquity, 0 eccentricity) over a 360-day year. All simulations have atmospheric CO₂ fixed at 300 ppm. The model is run using a T42 horizontal grid (~2.8°) and 40 vertical levels.

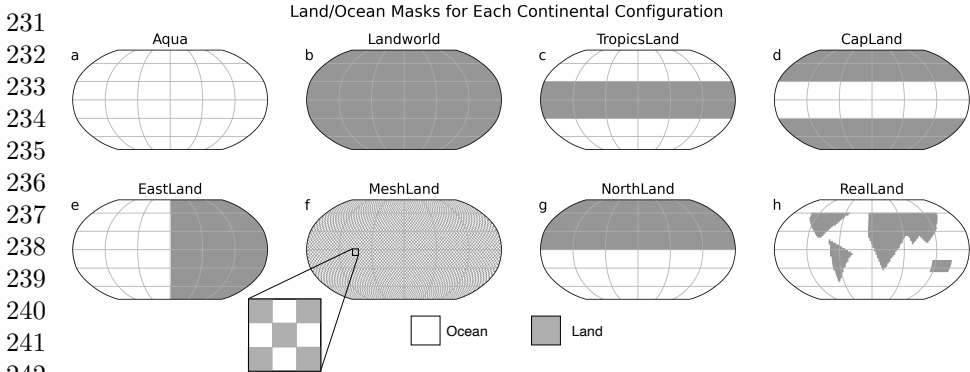
The atmosphere uses moist dynamics and produces precipitation, but does not represent the radiative effects of clouds. Therefore, we set the surface albedo of both water and land to a higher value than in a model that represents clouds, allowing for a more reasonable planetary albedo at the top of the atmosphere (see below for more details). In the configuration of the model used here, there are no albedo feedbacks from snow on land or sea ice. The Rapid Radiative Transfer Model (RRTM) (Vallis et al, 2018; Clough et al, 2005; Mlawer et al, 1997) is used for atmospheric radiative transfer, and we use the Simple Betts-Miller convection scheme (Betts, 1986; Betts and Miller, 1986; Frierson, 2007).

Analysis is primarily conducted using the Python programming language (Van Rossum and Drake, 2009), particularly with the NumPy (Harris et al, 2020), SciPy (Virtanen et al, 2020), and xarray (Hoyer and Hamman, 2017) packages.

2.2 Experiments

We run eight simulations, ranging from an all-ocean (Aqua) to an all-land (LandWorld) planet (Fig. 1). For five of the simulations, 50% of the planet's surface is covered by different distributions of land, and ocean covers the remaining 50% of the surface. TropicsLand has a single large continent in a belt around the equator, from 30°S to 30°N, with two oceans over each polar cap. CapLand is the inverse of this, with two continents capping the poles to 30°N/S, and a single large tropical ocean. NorthLand has a single large continent covering the whole northern hemisphere of the planet. EastLand has a single large continent covering the planet from the south to north poles, but only from 0-180°E longitude. In MeshLand, gridcells alternate between land and ocean in a checker-board pattern. Each patch of land/ocean in MeshLand is a single gridcell (roughly 2.8°). All simulations except RealLand have no orography. The RealLand simulation uses a semi-realistic, simplified continental configuration with roughly 20% of the surface covered by land, and idealized orographic representations of the Tibetan Plateau and the Rocky Mountains. This continental configuration is a modified version of that in Saulière et al (2012), and is produced using Isca's idealized land generator function (Vallis et al, 2018).

185
186
187
188
189
190
191
192
193
194
195
196
197
198
199
200
201
202
203
204
205
206
207
208
209
210
211
212
213
214
215
216
217
218
219
220
221
222
223
224
225
226
227
228
229
230



243 **Fig. 1** Land/ocean masks for each continental configuration. Ocean is shown in white; land
 244 is shown in grey. A small section of MeshLand (f) is enlarged to show the land/ocean tiling
 245 pattern, where each tile is one gridcell (at roughly 2.8° resolution).

246 Land differs from ocean in these simulations through its albedo, smaller
 247 heat capacity, fixed capacity to hold water, and increased resistance to evapo-
 248 ration under dry soil conditions (table 1). In our simulations, land is 1.3 times
 249 brighter than the ocean; the ocean has an albedo of 0.25 and the land an albedo
 250 of 0.325. This is brighter than typical albedo values for ocean (Jin et al, 2004)
 251 and (snow-free) land (Bonan, 2008), allowing the model to generate similar
 252 global mean surface temperatures to our modern climate without the radiative
 253 effects of clouds, which increase planetary albedo (Herman et al, 1980).
 254

255 **Table 1** Surface properties of land vs. ocean in all simulations

	Albedo	Capacity to hold water [mm]	Heat capacity in equivalent water depth [m]
Ocean	0.25	Unlimited	20
Land	0.325	150^1	2

263 [1] Except in the LandWorld simulation, where water is allowed to accumulate beyond 150 mm.

264

265 The land can hold up to 150 mm of water at each point, with soil moisture
 266 represented by bucket hydrology. Land is initialized with 100 mm of water
 267 at every land gridcell. When the bucket is less than 3/4 full, the evaporative
 268 resistance of the land surface increases linearly as a function of soil dryness.
 269 When the bucket is more than 3/4 full, the resistance to evaporating water
 270 from the land surface is the same as that over open water. Water in excess of the
 271 bucket capacity is discarded as runoff; in effect, it is immediately returned to
 272 the ocean. However, in LandWorld there is no ocean for runoff to be discarded
 273 to, nor is there an oceanic water source to replenish the atmosphere with
 274 water; thus, discarding runoff would result in a system that does not conserve
 275 water. To address this, hydrology on LandWorld is modified to allow for the
 276 formation of lakes: water is allowed to accumulate in excess of the 150mm

bucket capacity, with the evaporative resistance the same as that of open water until the amount of water in the gridcell drops back below 150mm, at which point the standard bucket hydrology rules apply. The atmospheric circulation of LandWorld rapidly transports all of the available moisture to the polar regions where the land forms two “lakes” (see [Laguë et al \(2021\)](#) for discussion of the formation of polar lakes on an all-land planet). Note that despite the implementation of lakes in the LandWorld simulation, there is still a slow leak of water vapor from the atmosphere which causes the simulation to cool over time (Fig. A1); this is a known bug of Isca that is apparent in all-land configurations (see <https://github.com/ExeClim/Isca/issues/177>) and is not evident in the other simulations which can continuously replenish water vapor from the oceans.

The aerodynamic roughness of the land and ocean are the same in these simulations because the effects of surface roughness are outside the focus of this study. In reality, land is typically more aerodynamically rough than the ocean; the implications of this for climate are explored by past studies ([Sud et al, 1988](#); [Davin et al, 2010](#); [Laguë et al, 2019](#)).

The ocean is represented with a 20m deep mixed layer ocean that allows sea surface temperatures to evolve. No lateral heat transport is prescribed in these simulations. The heat capacity of the land surface in these simulations is 1/10 that of the ocean, and corresponds to that of a 2m deep mixed layer ocean, a larger value than the heat capacity of typical land surfaces on the modern Earth. The land and ocean heat capacities were selected based on previous Isca simulations that generate realistic climatologies ([Thomson and Vallis, 2019](#); [Geen et al, 2018](#)).

Simulations are run for 20 years, with the first 4 years discarded to allow for model spin-up. After 4 years, global mean surface temperatures and average terrestrial soil moisture are stable for all simulations except LandWorld, which continues to lose water and cool throughout the length of the simulation (Fig. A1). Over the last decade of the LandWorld simulation, global mean temperatures decrease by roughly 1.5 K, but even without the water leak we expect this simulation to be cold and dry because the atmospheric circulation rapidly transports all the moisture to the polar regions where there is limited energy for evaporation.

3 Results & Discussion

3.1 Overview of scenarios

The eight different continental configurations considered here generate a wide variety of climates. The global average annual mean surface temperatures span almost 15 K (Fig. 2), ranging from the coldest global mean surface temperature on LandWorld (273.0 (± 1.2) K) to the warmest global mean surface temperature closely shared among RealLand (286.7 (± 0.03) K) and CapLand (286.5 (± 0.1) K; numbers in brackets show \pm the interannual standard deviation).

Table 2 Area in millions of km² (global and land-only) with annual mean temperature above 0°C ($T_{ANN} > 0^\circ\text{C}$), and with annual mean precipitation above 300 mm/year ($P_{ANN} > 300\text{mm/year}$). Also shown is the % of the total land on each planet meeting these criteria, and the equator to pole temperature difference in K for each continental configuration (noted separately for the northern and southern hemispheres for NorthLand and RealLand, which are not symmetric about the equator).

Continental Configuration	Total Area with $T_{ANN} > 0^\circ\text{C}$, in [km ² × 10 ⁶]	Land Area with $T_{ANN} > 0^\circ\text{C}$, in [km ² × 10 ⁶]	% of Land Area with $T_{ANN} > 0^\circ\text{C}$	Eq to Pole ΔT [K]	Total Area with $P_{ANN} > 300$ [mm/year], in [km ² × 10 ⁶]	Land Area with $P_{ANN} > 300$ [mm/year], in [km ² × 10 ⁶]	% of Land Area with $P_{ANN} > 300$ [mm/year]
Aqua	424	–	–	33	478	–	–
LandWorld	337	337	66	45	57	57	11
TropicsLand	378	260	100	34	273	64	25
CapLand	422	162	65	44	510	250	100
EastLand	396	193	76	43	322	85	33
MeshLand	416	205	80	36	492	244	96
NorthLand	406	188	74	46 (NH), 31 (SH)	432	189	74
RealLand	440	108	91	32 (NH), 29 (SH)	453	81	68

Over paleoclimate timescales, global mean temperatures are influenced by many factors, including changes in atmospheric CO₂ and ocean heat transport (Tierney et al, 2020). Our results show that continental distribution— independent of its impacts on CO₂ or ocean circulation—could be a potentially overlooked contributor to variations in past climate, as the range of surface temperatures generated solely by altering the continental arrangement and total amount of land produces changes in global mean surface temperature of the same order of magnitude as the temperature range experienced on Earth over the last 500 million years (Voosen, 2019).

The spatial distribution of surface temperatures varies between simulations (Fig. 2). The strongest equator-to-pole annual mean difference in surface temperature occurs over the continent in the NorthLand configuration, followed by LandWorld and CapLand, while the smallest equator-to-pole temperature difference occurs in both hemispheres of RealLand, followed by Aqua (Table 2).

Along with global temperature, the continental configurations also alter atmospheric circulation and global mean precipitation, with configurations with both more and less global mean rainfall than the modern Earth (Fig. 3). The highest global mean rain value occurs in the CapLand continental configuration (3.27 ± 0.01 mm/day), with the most rain falling over the tropical ocean. The lowest global mean precipitation values occur in Landworld (0.31 ± 0.16 mm/day).

All the continental configurations considered in this study can support liquid water, a common criteria for planetary habitability (Seager, 2013). However, the total area of land that would be hospitable to modern terrestrial ecosystems varies substantially across these continental configurations. To coarsely quantify the total land area in each simulation hospitable to modern day terrestrial ecosystems, we calculate the land area in each simulation with the annual mean temperature above freezing ($T_{ANN} > 0^\circ\text{C}$). We also calculate the land area with annual mean precipitation above 300 mm/year ($P_{ANN} > 300\text{mm/year}$), which roughly marks the divide between arid and semi-arid ecosystems (Salem, 1989).

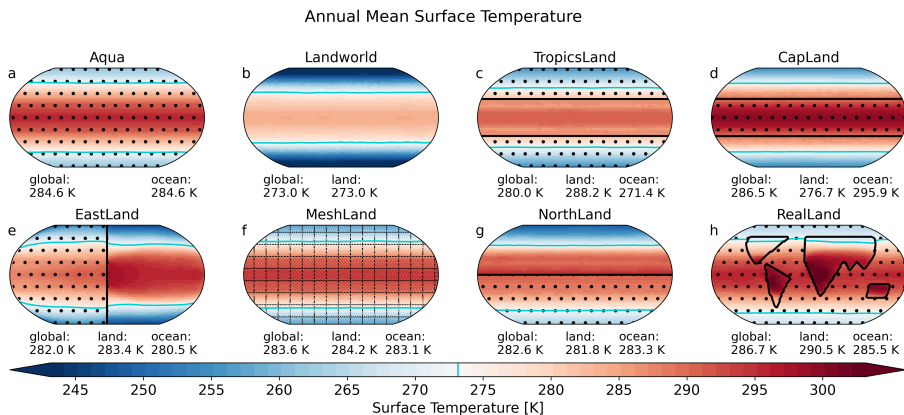


Fig. 2 Maps of annual mean surface temperature [K]. Ocean regions are stippled (except in MeshLand, where diagonal hatching is used to indicate the alternating land/ocean gridcells). Global, land-only, and ocean-only area-weighted annual mean values are noted below each map.

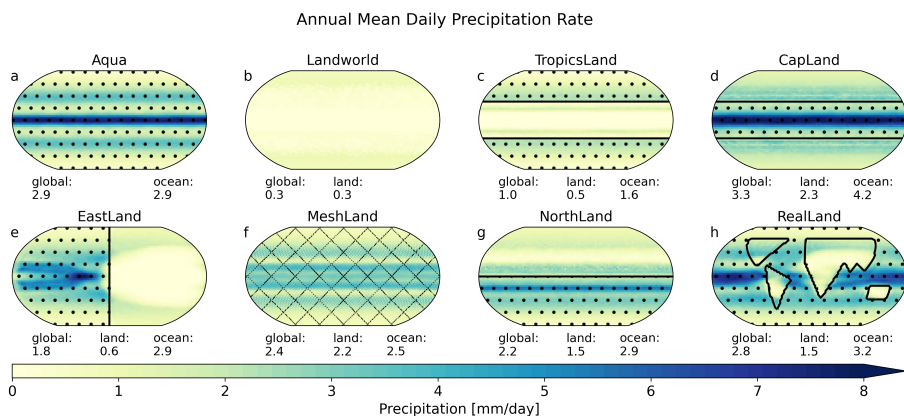


Fig. 3 Maps of annual mean precipitation [mm/day]. Ocean areas stippled (except in MeshLand, where diagonal hatching is used to indicate the alternating land/ocean gridcells). Global, land-only, and ocean-only area-weighted annual mean values are noted below each map.

The spread in the total land area with $T_{ANN} > 0^{\circ}\text{C}$ across simulations spans hundreds of millions of square kilometers (Table 2). RealLand has the smallest total land with $T_{ANN} > 0^{\circ}\text{C}$, but it also has the smallest amount of land to begin with. Of the 50/50 land/ocean planets, CapLand and NorthLand have the smallest land area with $T_{ANN} > 0^{\circ}\text{C}$, while TropicsLand and MeshLand have the most. LandWorld, which has the largest total land area, also has the largest amount of land above freezing in the annual average. However, both LandWorld and TropicsLand have large expanses of very dry land (Table 2). Indeed, only 11% of the land on LandWorld and 25% of the land on TropicsLand have $P_{ANN} > 300\text{mm/year}$. In contrast, 96% and 100% of

415 the land in MeshLand and CapLand (respectively) exceed the 300 mm/year
 416 precipitation threshold. Climate zone classifications provide a combined esti-
 417 mate of temperature and precipitation impacts on ecosystem distribution;
 418 Köppen-Geiger climate zones for each continental configuration explored here,
 419 calculated following [Kottek et al \(2006\)](#), are shown in Fig. A2.

420 In the sections below, we examine the main drivers of this wide spread
 421 in surface temperatures across the various continental arrangements, with
 422 particular focus on how land distribution impacts surface evaporation and
 423 atmospheric water vapor, the role of albedo, and feedbacks driven by dif-
 424 ferences in land vs. ocean heat capacity. The appendices contain figures
 425 showing transient and seasonal adjustments, meridionally resolved details, and
 426 additional fields of interest.

427

428 **3.2 Association of water vapor and the greenhouse effect** 429 **with surface temperatures**

430

431 The various continental configurations explored here have a strong control
 432 on surface evaporation, and thus on the concentration of atmospheric water
 433 vapor. We find that the impact of the continental configuration on water vapor
 434 is the dominant control driving the spread of global mean surface tempera-
 435 tures across simulations, while differences in albedo and absorbed shortwave
 436 radiation play a secondary role.

437 Continental configurations that allow for the largest globally averaged
 438 latent heat flux (evaporation) produce the warmest global mean surface tem-
 439 peratures (Fig. 4a). This contrasts with the intuition of evaporative cooling
 440 leading to cooler surface temperatures. There is a strong linear relationship
 441 ($r^2=0.87$) between the global mean values of surface temperature and sur-
 442 face latent heat flux. Configurations with high surface latent heat flux have
 443 high total column water vapor (Fig. 4b). However, given the temperature-
 444 dependence of water’s saturation vapor pressure, we must further explore this
 445 relationship to understand the cause and effect.

446 The total amount and spatial distribution of water vapor, a strong green-
 447 house gas, varies substantially across the continental configurations explored
 448 here (Figs. 4b, 5). All other greenhouse gases are prescribed to be identical
 449 across the simulations. We assess the effect of differences in water vapor con-
 450 centration by approximating the strength of the greenhouse effect (following
 451 [Kiehl and Trenberth \(1997\)](#)) as the difference between longwave (LW) radi-
 452 ation emitted at the surface and emitted at the top of the atmosphere (TOA;
 453 equation 1):

$$454 \quad LW_{diff} = LW_{surface}^{\uparrow} - LW_{TOA}^{\uparrow}. \quad (1)$$

455 Small values of LW_{diff} indicate a weak greenhouse effect while large values
 456 indicate a strong greenhouse effect.

457 Across the continental configurations tested, there are a wide variety of cli-
 458 mate states that fall along a common line relating evaporation, water vapor,
 459 and surface temperatures. A strong linear correlation ($r^2 = .82$) exists across
 460 continental configurations between globally averaged latent heat flux and

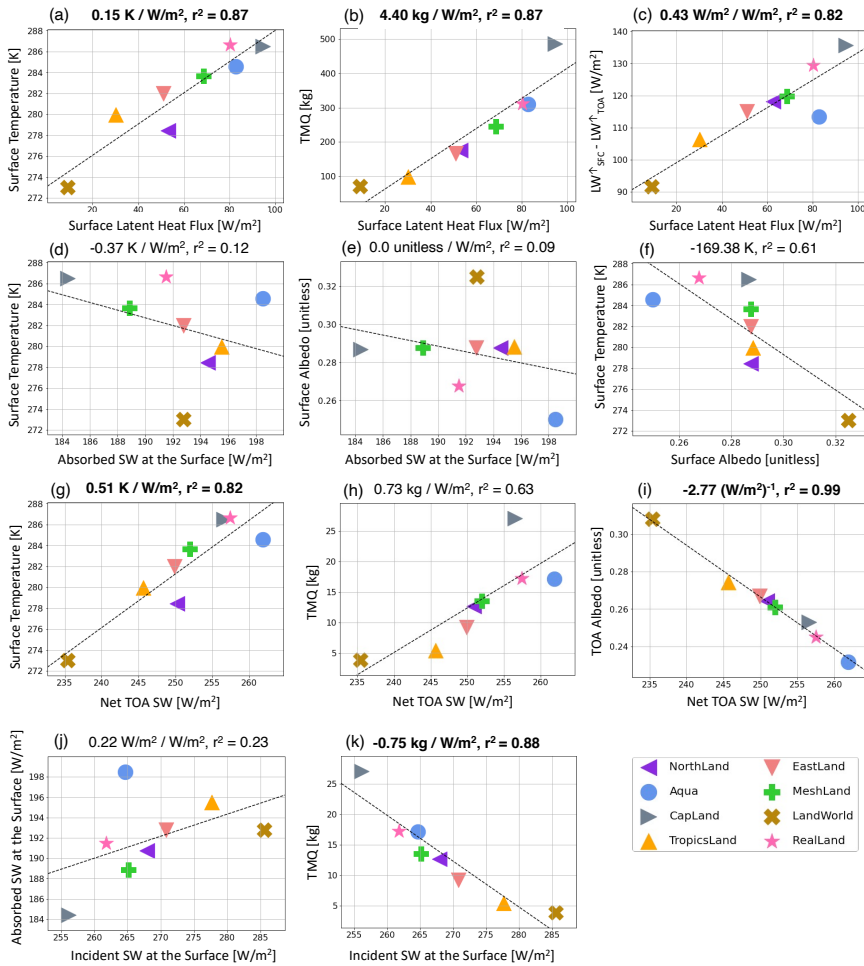


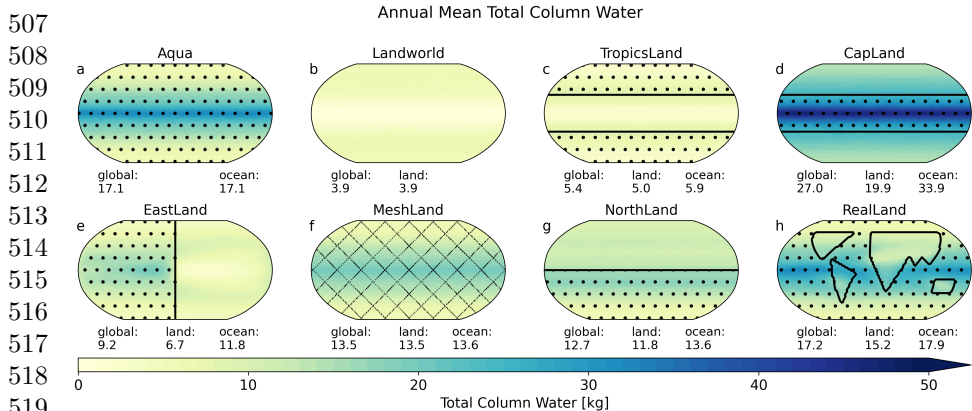
Fig. 4 Scatter plots showing the relationship between various global mean climate variables across the eight continental configurations. All values are shown for the annual mean, with each marker representing an individual continental configuration. The slope and r^2 value of a linear fit (dashed black line) is noted at the top of each panel, with slopes with a p-value < 0.05 shown in bold.

LW_{diff} , where configurations with high surface evaporation—and high water vapor (not shown)—have a stronger greenhouse effect (Fig. 4c). In the following sections, we discuss why each continental configuration leads to each distinct distribution of atmospheric water vapor and surface temperatures.

3.3 Surface albedo differences alone do not explain temperature spread

In our experimental planetary continental configurations, all planets that are 50% land and 50% ocean have the same globally averaged surface albedo. Yet,

461
462
463
464
465
466
467
468
469
470
471
472
473
474
475
476
477
478
479
480
481
482
483
484
485
486
487
488
489
490
491
492
493
494
495
496
497
498
499
500
501
502
503
504
505
506



520 **Fig. 5** Maps of climatological annual mean total atmospheric water vapor [kg] for each continental configuration. Ocean regions are indicated with black stippling, except in MeshLand where gridcells alternate between land and ocean (indicated by checked hatching, which is not to scale with the model's grid). Global, land-only, and ocean-only area-weighted annual mean values are noted below each map.

524
525
526
527 for the five continental configurations that are half land and half water and thus with identical surface albedos, there is a roughly 10 K spread in global mean surface temperature (Fig. 4e-g).

530 Planets with more water (Aqua and RealLand) have an overall darker surface while LandWorld has an overall brighter surface. Surface albedo determines how much of the shortwave radiation energy reaching the surface is absorbed at the planetary surface, and can play a role in controlling surface temperatures by modulating the total amount of energy available to the land surface. Because the model we use does not represent the radiative effects of clouds, we might expect surface albedo to have a stronger impact on top of atmosphere albedo—and thus climate—than in the modern Earth. However, we still see a large spread in the TOA albedo (as shown by the net shortwave radiation flux at the TOA; Fig. 4i), resulting from changes in water vapor.

540 Along with the surface albedo, the amount of incident shortwave radiation in a region also modulates how much shortwave radiation is available for absorption at the surface. Given the absence of clouds in our simulations, one might hypothesize for simulations with darker ocean near the tropics and brighter land near the poles to absorb more shortwave radiation than simulations with bright land in the tropics since more shortwave radiation is incident at the top of the atmosphere in the tropics than in the high latitudes. However, we find simulations with bright tropical land masses, including TropicsLand and LandWorld, absorb relatively high amounts of shortwave radiation at the surface (Fig. 4d,e). This apparent discrepancy between surface albedo and absorbed shortwave radiation results from more shortwave radiation reaching the surface in configurations with tropical land (Fig. 4h). Water vapor impacts both shortwave and longwave radiative transfer through the atmosphere, and

larger amounts of shortwave radiation reach the surface in TropicsLand and LandWorld because the atmosphere is very dry. 553
554

Top of atmosphere albedo plays a central role in modulating global climate (Donohoe and Battisti, 2011). As our simulations do not have clouds, top of atmosphere albedo is instead a function of surface albedo and water vapor concentrations. The large differences in water vapor across our simulations generate a spread in TOA albedo even among simulations with the same globally averaged surface albedo (Fig. 4f; note that we plot absorbed SW at TOA as a proxy for TOA albedo because all models have identical insolation). There is a correlation ($r^2 = 0.82$) between the globally averaged TOA absorbed SW and global mean surface temperatures, with continental configurations which absorb more net SW radiation at the TOA being generally warmer than configurations which absorb less net SW radiation at the TOA. However, TOA albedo alone does not explain the full spread in surface temperatures across continental configurations. For example, Aqua absorbs the most TOA SW (i.e. has the lowest TOA albedo), but both RealLand and CapLand are warmer. 555
556
557
558
559
560
561
562
563
564
565
566
567
568

Though the largest difference in surface albedo is between Aqua and LandWorld, their difference in globally averaged shortwave radiation absorbed at the surface is fairly small (Fig. 4e). That is, globally averaged surface albedo does not correlate well with globally averaged absorbed surface shortwave radiation. While the surface in LandWorld is much more reflective than the surface in Aqua, the dry atmosphere in LandWorld allows a larger amount of solar energy to reach the surface than the moist atmosphere of Aqua (Figs. 4j,k, 5b). Atmospheric water vapor both scatters and absorbs shortwave radiation (even in the absence of clouds), leading to less shortwave radiation incident upon the surface of Aqua than the surface of LandWorld. 569
570
571
572
573
574
575
576
577
578

For the 50/50 land/water planets, which all have the same surface albedo, there is about a 10 W/m² range in total absorbed shortwave radiation (SW) at the surface (Fig. 4e). RealLand, which has a smaller total land area, falls roughly in the middle of the spread. The reason for this non-intuitive relationship between global mean surface albedo and global mean absorbed shortwave radiation at the surface is the result of variations in incident shortwave radiation at the surface between continental configurations, which are due to differences in atmospheric water vapor concentrations. For example, CapLand absorbs a relatively small amount of globally averaged shortwave radiation despite the presence of dark ocean surface in the tropics. However, CapLand has a large concentration of atmospheric water vapor in the tropics (Fig. 5d) due to its tropical ocean. Because atmospheric water vapor scatters and absorbs shortwave radiation, there is less shortwave radiation incident upon the dark tropical surface in CapLand than there is in simulations with drier atmospheres, and thus less shortwave radiation is absorbed despite the dark tropical surface (Fig. 4j). TropicsLand, in comparison, has a much more reflective tropical surface than CapLand, but absorbs more total shortwave radiation because its dry atmosphere allows more solar energy to reach the surface than the humid atmosphere of CapLand. 579
580
581
582
583
584
585
586
587
588
589
590
591
592
593
594
595
596
597

598

599 Over sufficiently long timescales, the surface must balance the absorption
600 of shortwave energy either by heating up (and thus removing energy from
601 the surface as longwave radiation or sensible heat), or by evaporating water
602 (removing energy from the surface as latent heat). For land, this occurs on
603 comparatively short time scales due to its small heat capacity. The larger heat
604 capacity of the ocean allows it to absorb more shortwave energy before that
605 energy must be shed as latent heat, sensible heat, or longwave radiation. This
606 difference in heat capacity plays a critical role in explaining why CapLand is
607 both warmer and wetter than Aqua, which we discuss in section 3.6. In the
608 real ocean, heat can also be transported by the ocean circulation, but our
609 simulations have no ocean circulation by design. The sign of the relationship
610 between the amount of shortwave radiation absorbed at the surface and the
611 global mean surface temperature is the opposite of what one might naively
612 expect: the warmest climates are those that absorb the least amount of SW
613 radiation at the surface (Fig. 4d). Planets with less land (RealLand, Aqua)
614 fall above this line, while the planet with more land (LandWorld) falls below
615 this line.

616 LandWorld is colder than all the other continental configurations despite
617 the large amount of absorbed SW at the surface (Fig. 4d). CapLand, RealLand,
618 and Aqua span the full range of simulated globally mean absorbed shortwave
619 at the surface, yet these three continental configurations are the 3 warmest
620 planets, with similar global mean surface temperatures (roughly 285 K).

621 This disconnect between globally averaged surface albedo, absorbed SW at
622 the surface, and surface temperature implies that we cannot rely on the surface
623 albedo differences of land and water alone to explain the varied climates across
624 continental configuration. These simulations do not allow for cloud effects on
625 radiation; however, when cloud impacts on planetary albedo are taken into
626 consideration for the modern Earth, surface albedo contributes only a small
627 amount to the top of atmosphere albedo, which controls the total amount of
628 energy absorbed by the Earth system at any given location (Donohoe et al,
629 2013).

630

631 **3.4 Longitudinal distribution of land cools by limiting** 632 **evaporation over the Eastland super-continent** 633

634 The effect of continental arrangement on surface temperatures and climate
635 through water vapor vs. albedo is further demonstrated in the comparison of
636 MeshLand and EastLand. MeshLand and EastLand have the same amount of
637 land at each latitude. As such, they have the same latitudinal distribution of
638 surface albedo (or, equivalently, the same insolation-weighted surface albedo).
639 We find that differences in water vapor driven by differences in evaporation
640 are the dominant control making MeshLand a warmer planet than EastLand.

641 Despite MeshLand and EastLand having the same latitudinal distribution
642 of surface albedo, there is more shortwave radiation incident upon the sur-
643 face in Eastland, so more shortwave radiation is absorbed at the surface of
644 EastLand compared to Meshland (Fig. 6). If this were the dominant control

on surface climate, we would expect EastLand to be warmer than MeshLand. Instead, we see that MeshLand is warmer; this is a result of differences in the strength of the water vapor greenhouse effect between the two continental configurations.

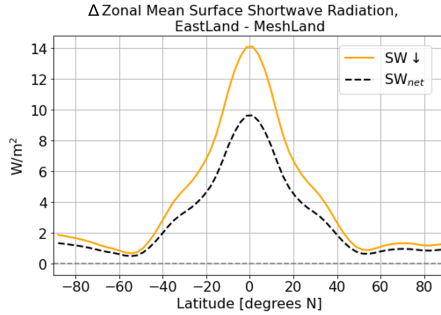


Fig. 6 Zonal mean, annually averaged difference in downwards (yellow) and net absorbed (black) shortwave radiation at the surface for EastLand - MeshLand.

The atmosphere in MeshLand has easy access to water everywhere, as each land gridcell is adjacent to ocean. In contrast, the atmosphere over the continent in EastLand is quite dry (c.f. Fig. 5e,f and A3e,f), particularly in the tropics where moisture that is advected onto the continent quickly precipitates out (Fig. 3e). The humid atmosphere of MeshLand results in a strong water vapor greenhouse effect, which drives the warmer temperatures of MeshLand compared to EastLand. This difference in water vapor also explains the difference in incident shortwave radiation between the two simulations; however, as noted above, this difference in shortwave radiation is not the controlling factor on surface temperature differences between these simulations.

Each MeshLand “island” behaves most similarly to archipelagos like the Maritime Continent, where the surrounding ocean provides moisture and the islands provide vertical motion for rainfall (Kooperman et al, 2017). Meanwhile, the zonal extent of the super continent of EastLand limits the range of moisture transport for precipitation to the interior, similar to Earth’s Asian continent (though more extreme). The resulting dry lands and overlying dry atmosphere of the EastLand super-continent cool the global climate.

In the idealized climate model used in these studies, there are no radiative effects of cloud cover. Cloud radiative effects are an important part of the climate system and can respond strongly to terrestrial processes (Cho et al, 2018; Sikma and Vilà-Guerau de Arellano, 2019; Laguë et al, 2019; Kim et al, 2020), but they also represent a large source of uncertainty (IPCC, 2013; Zelinka et al, 2017). While the radiative effects of clouds would play a role in the climate of all continental configurations considered here, they may be of particular importance in the comparison of MeshLand to EastLand. Specifically, we would expect MeshLand to be cloudy because its atmosphere has ample access to water everywhere and the smaller heat capacity of land would

691 result in larger sensible heat fluxes over the land than the neighbouring ocean
692 patches. This combination of vertical motion from sensible heating from the
693 land and a steady moisture supply from both the ocean and the wet land would
694 be conducive to the formation of cloud cover along the land/ocean boundary.
695 The entire planet of MeshLand is comprised of patchy islands—areas which, on
696 the modern Earth, enhance regional convection, cloud cover, and precipitation
697 (Cronin et al, 2015), such as occurs near the Maritime Continent.

698 The patchy nature of MeshLand’s continental distribution, and the result-
699 ing surface heat fluxes, is also reminiscent of regions of patchy deforestation
700 in the tropics. In the Amazon, deforestation on the scale of tens of km² has
701 been shown to lead to increased cloud cover at the grass-forest boundary. This
702 deforestation generates regional circulations driven by sensible heating over
703 the relatively dry grassland and moisture flux from the relatively moist rain-
704 forest (Khanna and Medvigy, 2014). Further exploration of a MeshLand-like
705 planet, potentially with land patches of varying size, in a model that allows
706 for radiatively interactive cloud cover would be useful to explore the impact
707 of coastal land on cloud formation at different latitudes.

708 Another process that strongly impacts cloud formation and precipitation
709 over complex topography is orographic lift (Kirshbaum and Smith, 2009;
710 Houze, 2012; Maroon et al, 2015). Elevated orography can drive circulations
711 and alter free-tropospheric temperature and regional climate, but the physics
712 of this are complex and interact strongly with surface albedo (Hu and Boos,
713 2017). With the exception of RealLand, which has a simplistic representation
714 of some mountain ranges, orographic effects are not represented in these flat-
715 land simulations. Rather than exploring the orographic effects of continents
716 on climate, here we are specifically focused on the differences in land vs. ocean
717 heat capacity, albedo, and evaporative properties and their effect on climate.

718

719 **3.5 Large tropical landmasses limit atmospheric water** 720 **vapor**

721

722 The coldest three simulations (LandWorld, Northland, and TropicsLand) all
723 have relatively large amounts of tropical land cover. These simulations are
724 colder than the others at most latitudes in the annual mean (Fig. 2 and A4).
725 Even EastLand, in which half of the tropics are covered by land, is cooler and
726 drier than the simulations with open water across the entire tropics. Land can
727 affect the global water vapor concentration both through evaporation and by
728 changing the saturation vapor pressure of the atmosphere through changes in
729 air temperatures.

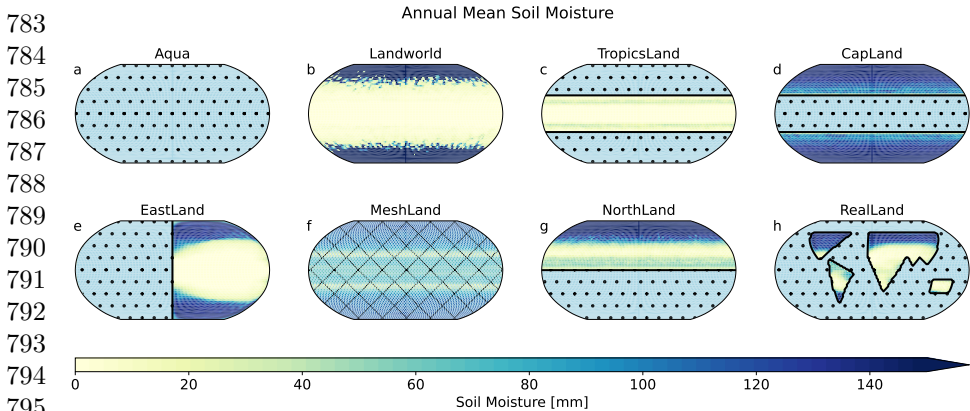
730 Albedo differences between land and ocean cannot explain why configura-
731 tions with large tropical land masses are cooler than other configurations. As
732 discussed in section 3.3, the total amount of shortwave radiation absorbed at
733 the surface is similar between these three simulations, and is higher than any
734 other planet except Aqua (Fig. 4). Low shortwave radiation absorption over
735 the tropical continents doesn’t explain the cooler global temperatures—thus
736 we examine differences in evaporation between simulations.

Generally, land is a dryer surface with limited water holding capacity compared to the ocean, and so serves to limit evaporation over the continents. The evaporative demand of the atmosphere is high in the tropics because of the warmer tropospheric air driven by high insolation. When there is ocean in the tropics, this evaporative demand is supplied by an effectively infinite reservoir of surface water. However, when the tropics are covered with land, the water on the land is quickly evaporated. While some of this moisture initially rains onto the land surface, e.g. in a classic intertropical convergence zone that occupies a narrow range of latitudes, tropical moisture export events (e.g. see Knippertz and Wernli, 2010) move moisture off the tropical continent. Eventually the tropical land dries out except along the edges of the continent, which experience seasonal precipitation.

The large latitudinal extent of the continent (between 30 degrees N-S) inhibits near-surface atmospheric moisture transport into the continental interior from the polar oceans. That is, were the equatorial continent of a smaller latitudinal extent, the equatorward component of the trade winds would travel over ocean (evaporating water along the way) before making landfall, thus bringing moisture onto the continent. With a latitudinally wide tropical continent, the near-surface winds travelling equatorward lie over land, thus the air is much drier than if the wind was travelling over an ocean surface. This results in most of the TropicsLand continent being dry, which means the tropical atmosphere cannot evaporate a large amount of moisture from the surface, resulting in a dry tropical atmosphere (Fig. A5).

In the modern continental configuration, near-surface winds in the tropics move moisture equatorward. However, in TropicsLand, the subsiding branch of the Hadley cell doesn't extend beyond the polar edge of the continent except in local summer. A small amount of moisture is brought onto the continental edge in summer (Fig. A5), but for the most part, surface winds in the low latitudes in TropicsLand do not travel over the ocean surface and thus do not transport moisture equatorward. In equilibrium, the large tropical land masses considered in this study are very dry and serve as a cap to tropical evaporation (Fig. 7).

Limited evaporation also means less latent cooling of the land surface, which could warm these tropical continents. However, the reduction of the water vapor greenhouse effect causes the continents to stay cool year round. The atmosphere at all latitudes becomes depleted in atmospheric water vapor (Fig. 5, A3). Instead of the surface temperature rising without evaporation, the atmosphere, robbed of its main source of moisture by the land surface, dries out and drives surface cooling via a reduced greenhouse effect. The weak greenhouse effect from low atmospheric water vapor is evident in the smaller magnitude of downwelling LW radiation at the surface in TropicsLand, LandWorld, and over the continent in Northland (Fig. A6). The water vapor feedback that operates in response to an arbitrary radiative forcing is expected to further reduce surface temperatures, amplifying the cooling produced by the initial land-induced drying.



796 **Fig. 7** Maps of annual mean soil moisture [mm]. Ocean areas are shown in light blue with
797 stippling (except in MeshLand, where diagonal hatching instead of stippling indicates the
798 alternating land/ocean gridcells). Note that all land regions have a maximum water-holding
799 capacity of 150 mm except LandWorld, which has been modified to allow for lake formation
800 to conserve water.

800

801

802

803 While there is ample water available for evaporation at higher latitudes—
804 e.g. over the polar oceans in TropicsLand, from high-latitude soil moisture
805 in NorthLand and Landworld, or from the southern hemisphere ocean in
806 NorthLand—the lack of energy for evaporation at higher latitudes and hori-
807 zontal mixing by the atmospheric circulation together maintain a dry tropical
808 atmosphere in these simulations. The mid-to-high latitude atmosphere in Trop-
809 icsLand does not contain nearly as much water vapor as the Aqua, CapLand,
810 MeshLand, or RealLand continental configurations (Figs. 5 and A3). The
811 southern hemisphere in NorthLand has much more water vapor than the north-
812 ern hemisphere, which is consistent with the warmer surface temperatures of
813 the southern hemisphere. The tradeoff between surface warming from reduced
814 evaporation and large-scale surface cooling from a reduced atmospheric water
815 vapor greenhouse effect is explored in detail for Northland in [Laguë et al](#)
816 ([2021](#)).

817 The colder climates seen in our simulations with extensive tropical land
818 cover may resemble Snowball Earth conditions, when tropical oceans were
819 hidden beneath sea glaciers ([Hoffman et al, 1998](#)), or during past geological
820 epochs when land was clustered into large tropical supercontinents ([Chandler](#)
821 [et al, 1992](#); [Merdith et al, 2021](#)). Though not explored here, we note that
822 differences in ocean dynamics on paleoclimate timescales can also be large
823 drivers of differences in climate even with approximately similar continental
824 configurations ([Chiang, 2009](#)).

825 In addition to their dry atmospheres, the atmospheric circulations of Land-
826 World, TropicsLand, and NorthLand differ drastically from those of the other
827 continental configurations. The meridional streamfunctions of the other conti-
828 nental configurations qualitatively resemble those of the modern Earth (Fig. 8).

However, for LandWorld, TropicsLand, and NorthLand, the dry tropical landmasses are highly depleted of soil moisture, and as such the tropical Hadley circulation is not dominated by moist dynamics, but rather by dry convection. The result is an overturning circulation which is vertically very short, and resembles the Hadley circulation expected for Snowball Earth (Voigt et al, 2012; Voigt, 2013) or the shallow meridional circulations over deserts (Zhai and Boos, 2017). In the case of NorthLand, this only applies to the northern hemisphere.

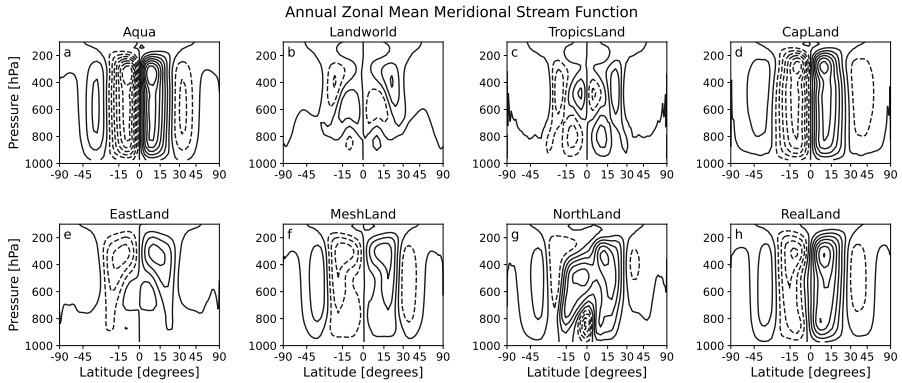


Fig. 8 Zonal mean meridional stream function annually averaged) for each continental configuration. Contours are spaced at 0.2×10^{11} kg/s. Solid contours indicate positive values (clockwise flow in this view) while dashed contours indicated negative values (counterclockwise flow).

3.6 Land heat capacity drives a seasonally asymmetric feedback with evaporation and water vapor

In this section, we focus on the differences between CapLand and Aqua, to explain why a planet that is 50% land covered is warmer and has more atmospheric water vapor than an aquaplanet where the entire planetary surface is ocean. The open tropical oceans in Aqua and CapLand result in these two simulations experiencing the most total evaporation and atmospheric water vapor of all our simulations (Figs. 4, 5). Note that in terms of global mean surface temperature, these simulations are the closest analogs to RealLand, which also has high surface evaporation and total atmospheric water vapor compared to other continental configurations.

The dark tropical ocean surface with effectively unlimited water for evaporation results in a moist tropical atmosphere for both CapLand and Aqua. Initially, water evaporated over the lower latitude ocean falls as precipitation on the equatorial edge of the polar continents of CapLand before it is evaporated again and transported by transient eddies to higher latitudes. Atmospheric moisture transport in CapLand provides enough water to maintain high soil moisture all year long (Figs. 7 and A7). We note, however, that

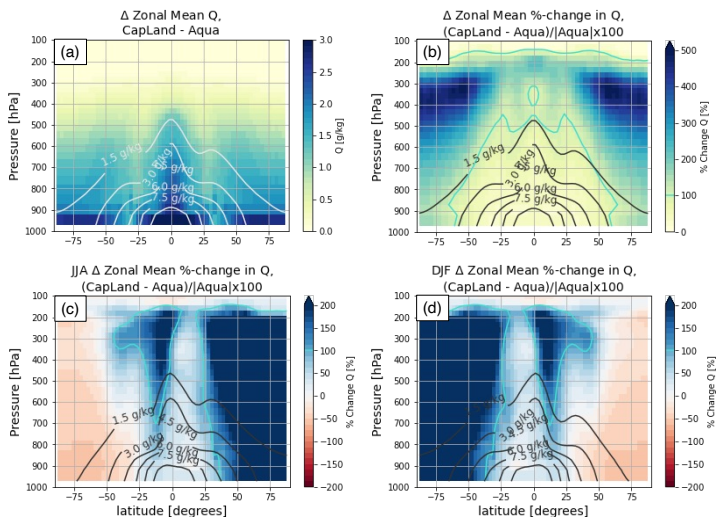


Fig. 9 Difference (CapLand – Aqua) in zonally averaged (a) annual mean specific humidity [g/kg] is shown in shading, with the climatological specific humidity [g/kg] from Aqua show in white contours. (b-c) show the percent change specific humidity for (b) the annual mean, (c) DJF, and (d) JJA in shading, with black contours showing climatological specific humidity [g/kg] from Aqua. Cyan contours in (b-d) show the 100% change in specific humidity line.

both CapLand and Aqua experience temperatures below freezing at the high latitudes during winter (Fig. A4), and thus we would expect the surface to be frozen for part of the year—but these simplified simulations do not account for the effects of sea ice or snow.

Despite its greater amount of land surface, CapLand is both warmer and has more atmospheric water vapor at all latitudes than Aqua (Fig. 9). This is particularly evident in the higher latitudes at higher levels of the troposphere, where the atmosphere in CapLand has over 100%—and in places in excess of 500%—more water vapor (in terms of specific humidity) than Aqua. While high soil moisture on the CapLand continents allows the surface to supply water to the atmosphere, the CapLand continent still differs from the high latitude ocean in Aqua in that it is brighter (higher albedo) and has a lower heat capacity.

The difference in both mean annual temperature and water vapor can be explained by the increased variation of seasonal temperature due to the land’s lower heat capacity and a seasonal feedback through water vapor. Over land, the smaller heat capacity results in a larger seasonal amplitude of temperature than over ocean. CapLand has seasonally warmer local summers and cooler winters over the polar continent than over the oceans at the same latitude in Aqua (Fig. 10c,d). This increase in amplitude is expected; however, an increase in the annual mean temperature is not.

To explain the observed increase in mean temperature, we must consider two factors: (i) energy can be shed from the land surface not only as long-wave radiation (LW), but also as sensible heat (SH) or evaporation/latent heat

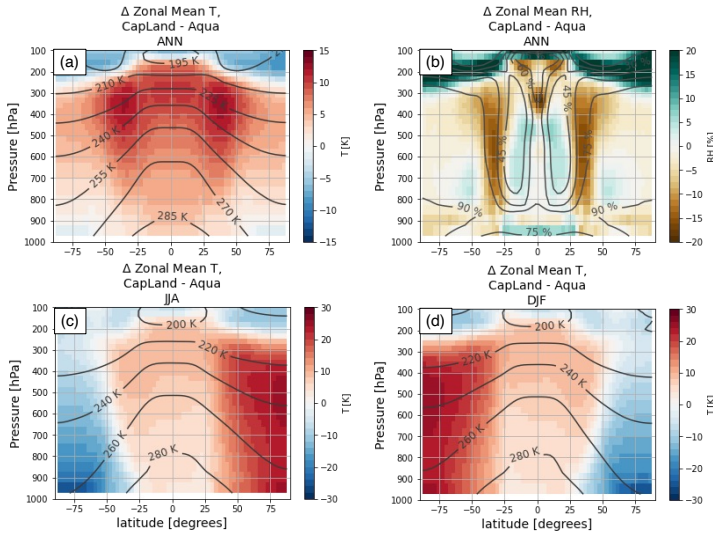


Fig. 10 Difference (CapLand – Aqua) in zonally averaged (a) annual mean air temperatures, (b) annual mean relative humidity, (c) DJF air temperatures and (d) JJA air temperatures, from the surface to 100 hPa. Contours show the climatological values for each field from the Aqua simulation.

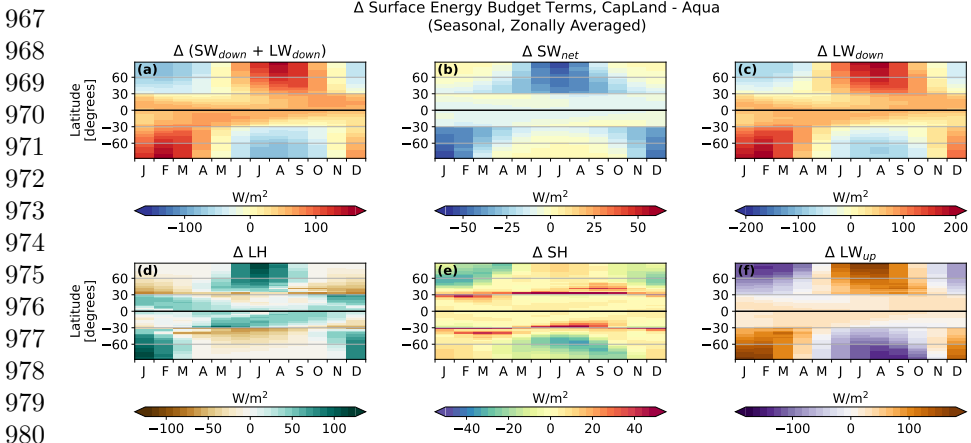
(LH), and (ii) feedbacks due to water vapor through the greenhouse effect and atmospheric energy transport. The seasonal imbalance between the local winter and summer is a result of a feedback between surface evaporation and the water vapor greenhouse effect.

During local summer, there is an increase in the total amount of radiative energy flowing into the land surface (SW + LW) in CapLand (Fig. 11a-c). This energy is shed from the land surface through a combination of increased surface temperatures (as evident by increased LW[↑] and SH), and increased surface evaporation (Fig. 11d-f). This leads to more atmospheric water vapor; because of the non-linearity of the Clausius Clapeyron relationship, the summer increase in specific humidity has a larger magnitude than the winter decrease (Fig. 9). Due to the increase in atmospheric water vapor during local summer, less incoming shortwave radiation reaches the surface (Fig. 11b). However, the increase in LW[↓] into the surface is much larger than this decrease in SW[↓] (Fig. 11a-c). The increase in LW[↓] is a result of higher atmospheric temperatures and increased atmospheric water vapor, leading to a stronger greenhouse effect (which also helps to increase atmospheric temperatures).

Increased LW[↓] into the surface adds energy into the land system, increasing the energy available for evaporation from the land. In CapLand, the soils remain wet through the summer (because of atmospheric moisture transport onto the continent; Figs. 7 and A7), supplying water to the hotter atmosphere and completing the feedback loop.

This evaporation-water vapor-greenhouse feedback is only possible *because* the continent in CapLand is very moist. Without available water on the polar

921
922
923
924
925
926
927
928
929
930
931
932
933
934
935
936
937
938
939
940
941
942
943
944
945
946
947
948
949
950
951
952
953
954
955
956
957
958
959
960
961
962
963
964
965
966



981 **Fig. 11** Hovmoller plots showing the seasonal cycle of the difference in zonally averaged
 982 surface energy fluxes between CapLand and Aqua. The total radiative energy flux into the
 983 surface is shown in (a), separated into the net absorbed SW in (b) and the downwelling
 984 LW in (c). Panels d-f show the fluxes of energy leaving the surface, as latent heat flux
 985 (evaporation) in (d), sensible heat flux in (e), and emitted longwave radiation in (f). Note
 986 the difference in the scale of the color bars between panels.

987

988 continents, the small heat capacity of land would lead to warming but no
 989 change in evaporation rates in summer. In this hypothetical dry polar land sce-
 990 nario, the water vapor–greenhouse feedback would be much weaker or would
 991 not occur at all. The moist polar continents buffer the summer surface temper-
 992 ature response as excess energy from the strengthened greenhouse effect goes
 993 into evaporating more water rather than into warming the surface, which fur-
 994 ther strengthens the greenhouse effect. There is very little change in sensible
 995 heat flux at the surface between CapLand and Aqua, except right along the
 996 continental boundary (Fig. 11e).

997 The increased energy into the surface, increased evaporation, stronger
 998 water vapor greenhouse effect, and the resulting increase in energy into the
 999 surface are specific to summer, and create a seasonal imbalance in atmospheric
 1000 air temperatures and atmospheric water vapor between summer and winter
 1001 on CapLand vs. Aqua. The atmosphere over the continent in CapLand dur-
 1002 ing local winter is slightly drier than the atmosphere over Aqua’s ocean at the
 1003 same latitude. In contrast, during local summer the atmosphere over CapLand
 1004 is much more humid than the atmosphere over Aqua’s ocean at the same lat-
 1005 itude (Fig. 10). Concurrently, the magnitude of warming in summer is larger
 1006 throughout the atmospheric column than the magnitude of cooling in winter.
 1007 Only at low altitudes above the land surface is the winter cooling compara-
 1008 ble to the summer warming in CapLand vs. Aqua (Figs. 10, 11f). The small
 1009 heat capacity of land interacting with the seasonal cycle drives this feedback,
 1010 which is why summer temperatures are amplified in CapLand vs. in Aqua.
 1011 This summertime CapLand-specific feedback does not occur in winter because
 1012 evaporation is low in both CapLand and Aqua.

The non-linear relationship between longwave radiation and surface temperature could also introduce seasonally asymmetric temperature responses, however in our simulations, this relationship fails to explain our results. If we were to assume that the difference in insolation between summer and winter must be removed from the land surface as longwave radiation through a change in surface temperature (i.e. ignoring sensible or latent heat flux) and that the change in insolation is equal and opposite in summer vs. winter, then by the Stefan–Boltzmann law ($LW \propto \sigma T^4$ (Stefan, 1879)), a *larger* change in surface temperature is needed during the cold season than is needed during the warm season in order to produce the same anomalous magnitude of longwave radiation. However, we do not find this in our simulations (Fig. 10c/d). Moreover, the critical difference in the CapLand vs. Aqua climate at high latitudes is the amplified amount of energy into the CapLand surface during local summer.

Past studies have explored similar idealized continental configurations to CapLand and TropicsLand, with opposing conclusions on which configuration makes for the warmer planet. Worsley and Kidder (1991) found that the tropical continental configuration allows for greater removal of CO₂ from the atmosphere through weathering and thus results in a cooler climate due to a diminished greenhouse effect. In contrast, Barron et al (1984) found the polar continental configuration generates the cooler climate as it provides a surface for high-latitude snow accumulation, which generates cooling through snow albedo feedbacks. In this study, we identify a third mechanism of importance: a planet with moist land capping the poles and a tropical ocean is warmer than the planet with a tropical land belt and polar oceans because the continental arrangement exerts strong controls on evaporation and atmospheric water vapor.

A critical difference between our simulations and those of Barron et al (1984) and Worsley and Kidder (1991) is our inclusion of a seasonal cycle. Without seasonality, the low heat capacity of land and the resulting summertime evaporation-water vapor-greenhouse effect feedback does not occur; this summertime warming feedback is the primary driver for our warmer CapLand simulation compared to Aqua. Moreover, our simulations do not allow for changing albedo from clouds, snow, or sea ice, nor changes in CO₂ due to weathering. Macdonald et al (2019) find arc-continent collisions in the low latitudes increase the removal of atmospheric CO₂ through intensified chemical weathering, a similar mechanism to that invoked by Worsley and Kidder (1991). However, the weathering mechanism requires the tropical continent to receive adequate moisture to allow for rock weathering. Yet our TropicsLand simulation provides a potential counterexample to this, where a large tropical land mass could have low weathering rates due to the dry atmosphere with limited precipitation. While we do not simulate rock weathering impacts on atmospheric CO₂ in our simulations, we would expect weathering rates to be lower over TropicsLand than, for example, MeshLand, which has much higher precipitation rates over land. That is, the intensity of weathering in the low

1059 latitudes requires not only the presence of land, but also the presence of pre-
1060 cipitation. However, if our tropical continent were smaller in extent, allowing
1061 for more atmospheric water vapor and precipitation, the potential for CO₂
1062 removal from rock weathering would likely be higher.

1063

1064

1065 4 Conclusions

1066

1067 The distribution of land exerts a first-order control on global climate by
1068 modulating atmospheric water vapor concentrations. The eight idealized con-
1069 tinental configurations considered here produced climates that span a range of
1070 roughly 15 K in global mean surface temperatures. We find strong relationships
1071 between surface evaporation, surface temperatures, and total atmospheric
1072 water vapor across the simulations.

1073 While the climate of each continental configuration considered here differs,
1074 the mechanisms controlling these climates share many commonalities; in par-
1075 ticular, each includes a feedback with the greenhouse effect of water vapor.
1076 When large landmasses are positioned in high insolation areas like the tropics,
1077 as is the case with TropicsLand, LandWorld, NorthLand, and EastLand, we do
1078 not get hot desert worlds; instead, the relatively dry land leads to water vapor
1079 depletion and a relatively cool climate. Our modern continental configuration
1080 drives a climate that is among the warmest and wettest of the configurations
1081 explored here, which is consistent with our findings that continental configu-
1082 rations with large tropical ocean area have warm, moist atmospheres. While
1083 there is land at low latitudes on modern Earth, there is also extensive ocean
1084 area; the relatively wet atmosphere of RealLand suggests that the modern
1085 Earth continental configuration does not limit tropical evaporation or tropical
1086 atmospheric water vapor.

1087 Also of great importance is the fact that the low heat capacity of a wet
1088 continent at the poles in CapLand creates a larger seasonal cycle of tempera-
1089 ture and generates a seasonal evaporation/water vapor feedback that amplifies
1090 summer warming. This feedback creates a climate that is wetter and warmer
1091 on a planet with 50% land cover than on an aquaplanet without continents.

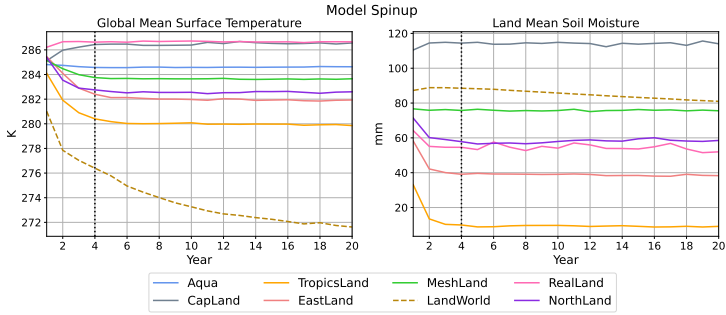
1092 Our framework allows us to isolate a new mechanism through which tropi-
1093 cal vs. extratropical land masses can modulate global-scale climate, and
1094 also highlights the importance of continental distribution for global climate
1095 through its influence on atmospheric water vapor. Further study is required
1096 to determine the combined climate effects of tropical vs. extratropical land
1097 on long-term atmospheric CO₂ concentrations, surface albedo (through snow
1098 cover), and top-of-atmosphere albedo (through cloud cover and water vapor
1099 effects). How much these various effects may amplify, damp, or generate
1100 interactions which could further feed back on global climate is necessary to
1101 understand the total impact of continental distribution on global-scale climate.

1102 The different continental configurations explored here are idealizations, but
1103 provide possible analogues for past continental configurations (see [Mer-
1104 et al \(2021\)](#)), or configurations on different water-land planets. We show how

the distribution of land on a planet's surface has a fundamental control on 1105
surface climate by modulating atmospheric water vapor concentrations and 1106
creating feedbacks between heat capacity and the seasonal cycle, with varia- 1107
tions in the distribution of a fixed amount of land across the planetary surface 1108
generating a substantial spread in global mean surface climate. 1109

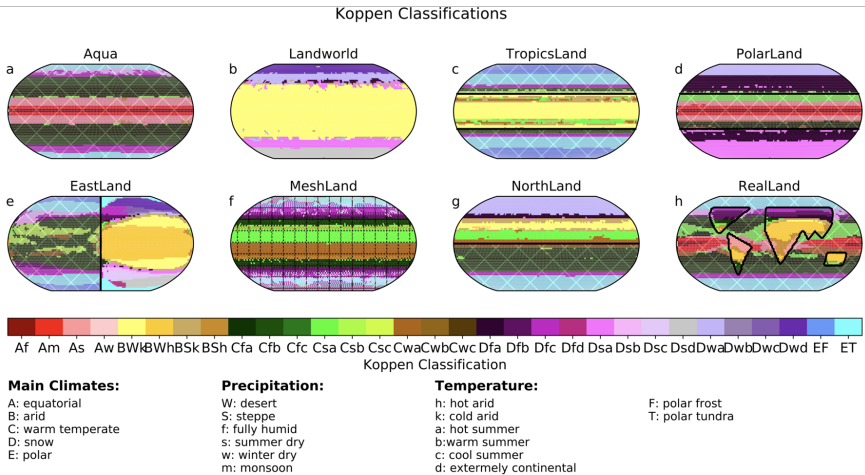
1110
1111
1112
1113
1114
1115
1116
1117
1118
1119
1120
1121
1122
1123
1124
1125
1126
1127
1128
1129
1130
1131
1132
1133
1134
1135
1136
1137
1138
1139
Acknowledgments. This research used the Savio computational cluster 1140
resource provided by the Berkeley Research Computing program at the Uni- 1141
versity of California, Berkeley (supported by the UC Berkeley Chancellor, 1142
Vice Chancellor for Research, and Chief Information Officer). Th is research 1143
used resources of the National Energy Research Scientific Computing Center 1144
(NERSC), a U.S. Department of Energy Office of Science User Facility located 1145
at Lawrence Berkeley National Laboratory, operated under Contract No. DE- 1146
AC02-05CH11231. We acknowledge high-performance computing support for 1147
analysis using the Casper platform of Cheyenne (doi:10.5065/D6RX99HX) 1148
provided by NCAR's Computational and Information Systems Laboratory, 1149
sponsored by the National Science Foundation. 1150

1151 **Appendix A Spinup & Additional Fields of Interest**
 1152
 1153
 1154
 1155
 1156



1167 **Fig. A1** Annual mean (a) global-mean surface temperature [K] and (b) land-mean soil
 1168 moisture (water in soil “bucket”, in [mm]) for each model simulation, showing equilibration
 1169 within 4 years of initialization for all simulations except LandWorld (dashed tan line). The
 1170 vertical dotted at year 4 marks the end of the spin-up period; model output up to and
 1171 including year 4 are discarded from the analysis in this study.

1172
 1173
 1174
 1175
 1176
 1177



1192 **Fig. A2** Köppen-Geiger climate zones for each continental configuration, calculated fol-
 1193 lowing Kottek et al (2006).

1194
 1195
 1196

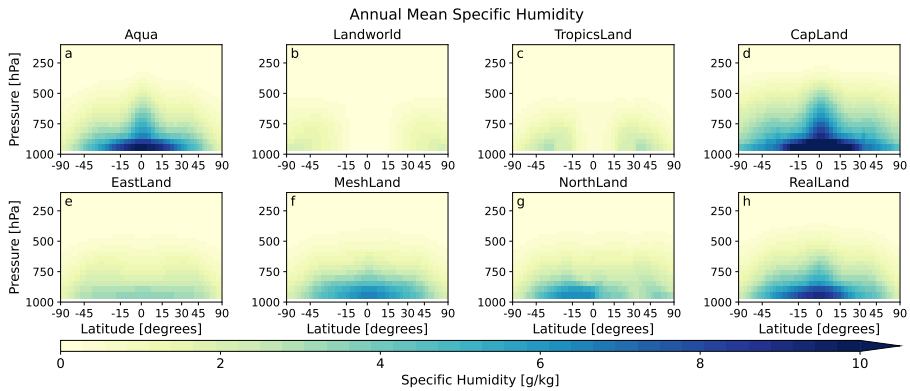


Fig. A3 Zonally averaged annual mean specific humidity from the surface to 100 hPa for each continental configuration.

Appendix B Transient and seasonal adjustments

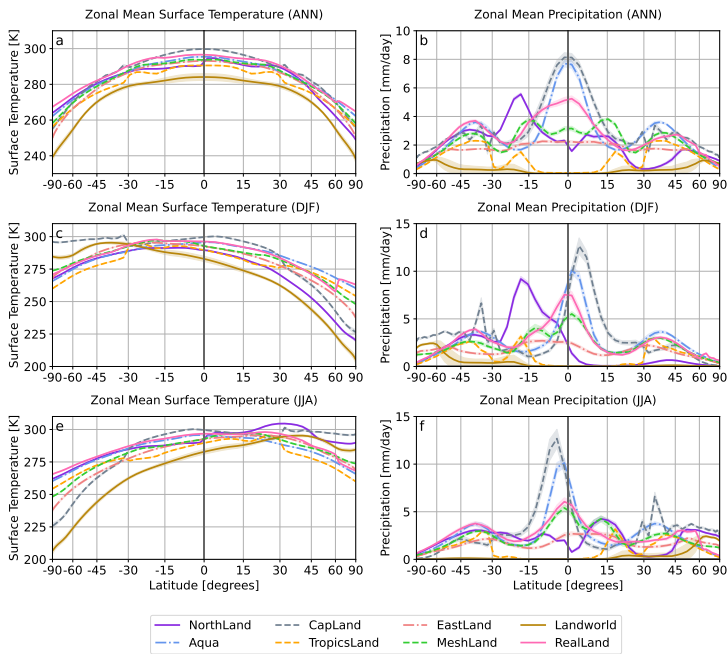
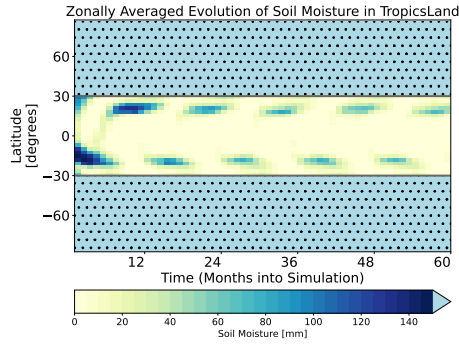


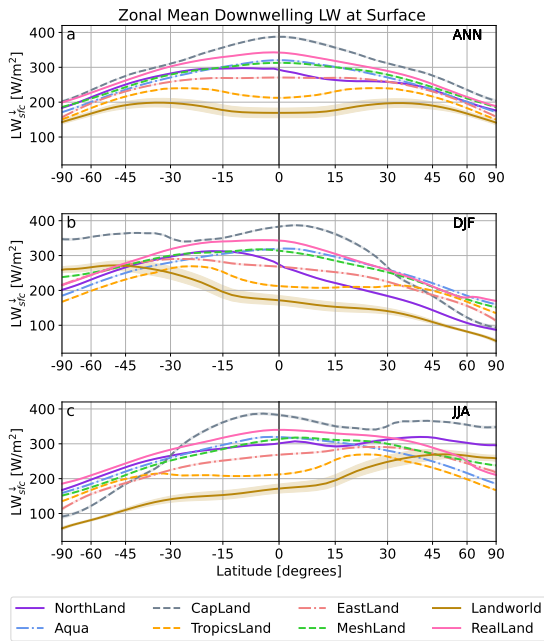
Fig. A4 Zonally averaged surface temperature (left) and precipitation (right) for each simulation in the annual mean (top), DJF (middle) and JJA (bottom).

1243
 1244
 1245
 1246
 1247
 1248
 1249
 1250
 1251
 1252
 1253
 1254
 1255



1256 **Fig. A5** Hovmöller plot showing the evolution of zonally averaged soil moisture for the
 1257 first five years of the TropicsLand simulation [mm]. Ocean areas are indicated by light blue
 1258 shading with stippling.

1259
 1260
 1261
 1262
 1263
 1264
 1265
 1266
 1267
 1268
 1269
 1270
 1271
 1272
 1273
 1274
 1275
 1276
 1277
 1278
 1279
 1280
 1281
 1282
 1283



1284 **Fig. A6** Zonally averaged downwelling longwave radiation at the surface (LW_{sfc}^{\downarrow} , in
 1285 W/m^2) for (a) the annual mean, (b) December-January-February, and (c) June-July-August
 1286 for each continental configuration. Shading indicates $\pm 1\sigma$ of interannual variability.

1287
 1288

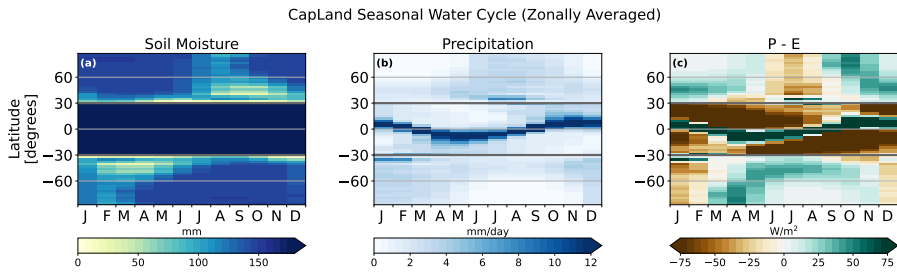


Fig. A7 Zonally averaged (a) soil moisture [mm], (b) precipitation [mm/day], and (c) precipitation-evaporation [W/m^2] over the course of the year for the CapLand simulation. Dark gray lines at 30° N/S indicate the continental/ocean boundary.

1289
 1290
 1291
 1292
 1293
 1294
 1295
 1296
 1297
 1298
 1299
 1300
 1301
 1302
 1303
 1304
 1305
 1306
 1307
 1308
 1309
 1310
 1311
 1312
 1313
 1314
 1315
 1316
 1317
 1318
 1319
 1320
 1321
 1322
 1323
 1324
 1325
 1326
 1327
 1328
 1329
 1330
 1331
 1332
 1333
 1334

1335 **Declarations**

1336
1337 **Ethical Approval.** Not applicable.

1338
1339
1340
1341
1342
1343

1344 **Competing Interests.** The authors have no relevant financial or non-
1345 financial interests to disclose.

1346
1347
1348
1349
1350
1351

1352 **Author Contributions.** Marysa M. Laguë designed the study, conducted
1353 the simulations, and conducted the analysis. Marysa M. Laguë and Sarah
1354 Ragen discussed the preliminary concept of the study. Marysa M. Laguë, Gre-
1355 gory R. Quetin, and William R. Boos discussed results and further analysis.
1356 Sarah Ragen conducted the literature review. The first draft of the manuscript
1357 was written by Marysa M. Laguë and all authors contributed to and com-
1358 mented on intermediate versions of the manuscript. All authors read and
1359 approved the final manuscript.

1360
1361
1362
1363
1364
1365
1366

1367 **Funding.** M.M.L. acknowledges funding support from the James S. McDon-
1368 nell Foundation Postdoctoral Fellowship in Dynamic and Multiscale Systems. SR
1369 acknowledges support from NSF Award OCE-1850900.

1370
1371
1372
1373
1374
1375

1376 **Data Availability.** Isca is publicly available on github at [https://](https://github.com/ExeClim/Isca)
1377 github.com/ExeClim/Isca. The specific version of Isca used in this study is
1378 archived on zenodo and github with the DOI 10.5281/zenodo.6800218. The
1379 analysis code, output from model simulations, python driver scripts, and
1380 modifications to the source code used in this study are publicly archived on
zenodo with the DOIs 10.5281/zenodo.7964297 and 10.5281/zenodo.7754428 .

References

- Baldocchi DD, Vogel CA, Hall B (1997) Seasonal variation of energy and water vapor exchange rates above and below a boreal jack pine forest canopy generally less than one-half was wet , daily evaporation. *Journal of Geophysical Research* 102(96):28,928–939,951. <https://doi.org/10.1029/96JD03325>
- Baross JA, Benner SA, Cody GD, et al (2007) *The Limits of Organic Life in Planetary Systems*. National Academies Press, Washington, DC, <https://doi.org/10.17226/11919>
- Barron EJ, Thompson SL, Hay WW (1984) Continental distribution as a forcing factor for global-scale temperature. *Nature* 310(5978):574–575. <https://doi.org/10.1038/310574a0>
- Barsugli J, Shin SI, Sardeshmukh PD (2005) Tropical climate regimes and global climate sensitivity in a simple setting. *Journal of the Atmospheric Sciences* 62(4):1226–1240. <https://doi.org/10.1175/JAS3404.1>
- Betts AK (1986) A new convective adjustment scheme. Part I: Observational and theoretical basis. *Quarterly Journal of the Royal Meteorological Society* 112(473):677–691. <https://doi.org/10.1002/qj.49711247307>
- Betts AK, Miller MJ (1986) A new convective adjustment scheme. Part II: Single column tests using GATE wave, BOMEX, ATEX and arctic air-mass data sets. *Quarterly Journal of the Royal Meteorological Society* 112(473):693–709. <https://doi.org/10.1002/qj.49711247308>
- Bonan GB (2008) Forests and climate change: Forcings, feedbacks, and the climate benefits of forests. *Science (New York, NY)* 320(5882):1444–1449. <https://doi.org/10.1126/science.1155121>
- Budyko MI (1961) The Heat Balance of the Earth's Surface. *Soviet Geography* 2(4):3–13. <https://doi.org/10.1080/00385417.1961.10770761>
- Budyko MI (1969) The effect of solar radiation variations on the climate of the Earth. *Tellus* 21(5):611–619. <https://doi.org/10.3402/tellusa.v21i5.10109>
- Burke CJ, Christiansen JL, Mullally F, et al (2015) TERRESTRIAL PLANET OCCURRENCE RATES for the KEPLER GK DWARF SAMPLE. *Astrophysical Journal* 809(1):8. <https://doi.org/10.1088/0004-637X/809/1/8>
- Cess RD, Goldenberg SD (1981) The effect of ocean heat capacity upon global warming due to increasing atmospheric carbon dioxide. *Journal of Geophysical Research* 86(80):498–502

- 1427 Chandler MA, Rind D, Ruedy R (1992) Pangaeian climate during the early
 1428 Jurassic: GCM simulations and the sedimentary record of paleoclimate. *Geo-*
 1429 *logical Society of America Bulletin* 104(5):543–559. [https://doi.org/10.1130/](https://doi.org/10.1130/0016-7606(1992)104(0543:PCDTEJ)2.3.CO;2)
 1430 [0016-7606\(1992\)104\(0543:PCDTEJ\)2.3.CO;2](https://doi.org/10.1130/0016-7606(1992)104(0543:PCDTEJ)2.3.CO;2)
 1431
- 1432 Charney J, Stone PH, Quirk WJ (1975) Drought in Sahara - Biogeophysical
 1433 Feedback Mechanism. *Science* 187(4175):434–435. [https://doi.org/doi:](https://doi.org/doi:10.1126/science.187.4175.434)
 1434 [10.1126/science.187.4175.434](https://doi.org/doi:10.1126/science.187.4175.434)
 1435
- 1436 Chiang JC (2009) The tropics in paleoclimate. *Annual Review of Earth*
 1437 *and Planetary Sciences* 37:263–297. [https://doi.org/10.1146/annurev.earth.](https://doi.org/10.1146/annurev.earth.031208.100217)
 1438 [031208.100217](https://doi.org/10.1146/annurev.earth.031208.100217)
 1439
- 1440 Cho MH, Yang AR, Baek EH, et al (2018) Vegetation-cloud feedbacks to future
 1441 vegetation changes in the Arctic regions. *Climate Dynamics* 50(9-10):3745–
 1442 3755. <https://doi.org/10.1007/s00382-017-3840-5>
 1443
- 1444 Clough SA, Shephard MW, Mlawer EJ, et al (2005) Atmospheric radiative
 1445 transfer modeling: A summary of the AER codes. *Journal of Quantita-*
 1446 *tive Spectroscopy and Radiative Transfer* 91(2):233–244. [https://doi.org/](https://doi.org/10.1016/j.jqsrt.2004.05.058)
 1447 [10.1016/j.jqsrt.2004.05.058](https://doi.org/10.1016/j.jqsrt.2004.05.058)
- 1448 Cronin TW, Emanuel KA, Molnar P (2015) Island precipitation enhancement
 1449 and the diurnal cycle in radiative-convective equilibrium. *Quarterly Journal*
 1450 *of the Royal Meteorological Society* 141(689):1017–1034. [https://doi.org/10.](https://doi.org/10.1002/qj.2443)
 1451 [1002/qj.2443](https://doi.org/10.1002/qj.2443)
 1452
- 1453 Davin EL, de Noblet-Ducoudré N, de Noblet-Ducoudre N, et al (2010)
 1454 Climatic Impact of Global-Scale Deforestation: Radiative versus Nonradia-
- 1455 tive Processes. *Journal of Climate* 23(1):97–112. [https://doi.org/10.1175/](https://doi.org/10.1175/2009JCLI3102.1)
 1456 [2009JCLI3102.1](https://doi.org/10.1175/2009JCLI3102.1)
 1457
- 1458 Dirmeyer PA (1998) Land-sea geometry and its effect on monsoon circulations.
 1459 *Journal of Geophysical Research Atmospheres* 103(D10):11,555–11,572.
 1460 <https://doi.org/10.1029/98JD00802>
 1461
- 1462 Donohoe A, Battisti DS (2011) Atmospheric and surface contributions to
 1463 planetary albedo. *Journal of Climate* 24(16):4402–4418. [https://doi.org/10.](https://doi.org/10.1175/2011JCLI3946.1)
 1464 [1175/2011JCLI3946.1](https://doi.org/10.1175/2011JCLI3946.1)
 1465
- 1466 Donohoe A, Marshall J, Ferreira D, et al (2013) The relationship between ITCZ
 1467 location and cross-equatorial atmospheric heat transport: From the seasonal
 1468 cycle to the Last Glacial Maximum. *Journal of Climate* 26(11):3597–3618.
 1469 <https://doi.org/10.1175/JCLI-D-12-00467.1>
 1470
- 1471 Eliassen A, Palm E (1960) On the Transfer of Energy in Stationary Mountain
 1472 Waves. *Geofysiske Publikasjoner*

- Enderton D, Marshall J (2009) Explorations of Atmosphere–Ocean–Ice Climates on an Aquaplanet and Their Meridional Energy Transports. *Journal of the Atmospheric Sciences* 66(6):1593–1611. <https://doi.org/10.1175/2008JAS2680.1>
- Fajber R, Kushner PJ (2021) Using ‘heat tagging’ to understand the remote influence of atmospheric diabatic heating through long-range transport. *Journal of the Atmospheric Sciences* <https://doi.org/10.1175/JAS-D-20-0290.1>
- Ferrari R, Ferreira D (2011) What processes drive the ocean heat transport? *Ocean Modelling* <https://doi.org/10.1016/j.ocemod.2011.02.013>
- Ferreira D, Marshall J, Campin JM (2010) Localization of deep water formation: Role of atmospheric moisture transport and geometrical constraints on ocean circulation. *Journal of Climate* 23(6):1456–1476. <https://doi.org/10.1175/2009JCLI3197.1>
- Frierson DM (2007) The dynamics of idealized convection schemes and their effect on the zonally averaged tropical circulation. *Journal of the Atmospheric Sciences* 64(6):1959–1974. <https://doi.org/10.1175/JAS3935.1>
- Geen R, Lambert FH, Vallis GK (2018) Regime change behavior during Asian monsoon onset. *Journal of Climate* 31(8):3327–3348. <https://doi.org/10.1175/JCLI-D-17-0118.1>
- Harris CR, Millman KJ, van der Walt SJ, et al (2020) Array programming with NumPy. *Nature* 585(7825):357–362. <https://doi.org/10.1038/s41586-020-2649-2>
- Held IM (1985) Pseudomomentum and the orthogonality of modes in shear flows. *Journal of the Atmospheric Sciences* 42(21):2280–2288. [https://doi.org/10.1175/1520-0469\(1985\)042<2280:PATOOM>2.0.CO;2](https://doi.org/10.1175/1520-0469(1985)042<2280:PATOOM>2.0.CO;2)
- Held IM, Ting M, Wang H (2002) Northern winter stationary waves: Theory and modeling. *Journal of Climate* 15(16):2125–2144. [https://doi.org/10.1175/1520-0442\(2002\)015<2125:NWSWTA>2.0.CO;2](https://doi.org/10.1175/1520-0442(2002)015<2125:NWSWTA>2.0.CO;2)
- Herman GF, Wu MLC, Johnson WT (1980) The Effect of Clouds on the Earth’s Solar and Infrared Radiation Budgets. *Journal of the Atmospheric Sciences* 37(June):1251–1261
- Hoffman PF, Schrag DP (2002) The snowball Earth hypothesis: Testing the limits of global change. *Terra Nova* 14(3):129–155. <https://doi.org/10.1046/j.1365-3121.2002.00408.x>

- 1519 Hoffman PF, Kaufman AJ, Halverson GP, et al (1998) A Neoproterozoic Snow-
1520 ball Earth. *Science* 281(5381):1342–1346. [https://doi.org/10.1126/science.](https://doi.org/10.1126/science.281.5381.1342)
1521 [281.5381.1342](https://doi.org/10.1126/science.281.5381.1342)
- 1522
1523 Hoffman PF, Abbot DS, Ashkenazy Y, et al (2017) Snowball Earth cli-
1524 mate dynamics and Cryogenian geology-geobiology. *Science Advances* 3(11).
1525 <https://doi.org/10.1126/sciadv.1600983>
- 1526
1527 Houze RA (2012) Orographic effects on precipitating clouds. *Reviews of*
1528 *Geophysics* 50(1):1–47. <https://doi.org/10.1029/2011RG000365>
- 1529
1530 Hoyer S, Hamman J (2017) Xarray: N-D labeled arrays and datasets in Python.
1531 *Journal of Open Research Software* 5(1). <https://doi.org/10.5334/jors.148>
- 1532
1533 Hu S, Boos WR (2017) The physics of orographic elevated heating in radiative-
1534 convective equilibrium. *Journal of the Atmospheric Sciences* 74(9):2949–
1535 2965. <https://doi.org/10.1175/JAS-D-16-0312.1>
- 1536
1537 Hui KL, Bordoni S (2021) Response of monsoon rainfall to changes in the
1538 latitude of the equatorward coastline of a zonally symmetric continent. *Jour-*
1539 *nal of the Atmospheric Sciences* 78(5):1429–1444. [https://doi.org/10.1175/](https://doi.org/10.1175/JAS-D-20-0110.1)
1540 [JAS-D-20-0110.1](https://doi.org/10.1175/JAS-D-20-0110.1)
- 1541
1542 IPCC (2013) Climate Change 2013 The Physical Change Basis. Climate
1543 Change 2013: The Physical Science Basis Contribution of Working Group I
1544 to the Fifth Assessment Report of the Intergovernmental Panel on Climate
1545 Change <https://doi.org/10.1017/CBO9781107415324>
- 1546
1547 Jin Z, Charlock TP, Smith WL, et al (2004) A parameterization of ocean
1548 surface albedo. *Geophysical Research Letters* 31(22):1–4. [https://doi.org/](https://doi.org/10.1029/2004GL021180)
1549 [10.1029/2004GL021180](https://doi.org/10.1029/2004GL021180)
- 1550
1551 Kang SM, Held IM, Frierson DMW, et al (2008) The Response of the ITCZ
1552 to Extratropical Thermal Forcing: Idealized Slab-Ocean Experiments with
1553 a GCM. *Journal of Climate* 21(14):3521–3532. [https://doi.org/10.1175/](https://doi.org/10.1175/2007JCLI2146.1)
1554 [2007JCLI2146.1](https://doi.org/10.1175/2007JCLI2146.1)
- 1555
1556 Kang SM, Frierson DMW, Held IM (2009) The Tropical Response to Extrat-
1557 ropical Thermal Forcing in an Idealized GCM: The Importance of Radiative
1558 Feedbacks and Convective Parameterization. *Journal of the Atmospheric*
Sciences 66(9):2812–2827. <https://doi.org/10.1175/2009JAS2924.1>
- 1559
1560 Khanna J, Medvigy D (2014) Strong control of surface roughness vari-
1561 ations on the simulated dry season regional atmospheric response to
1562 contemporary deforestation in Rondônia, Brazil. *Journal of Geophysical*
1563 *Research D: Atmospheres* 119(23):13,067–13,078. [https://doi.org/10.1002/](https://doi.org/10.1002/2014JD022278)
1564 [2014JD022278](https://doi.org/10.1002/2014JD022278)

- Kiehl JT, Trenberth KE (1997) Earth's annual global mean energy budget. *Bulletin of the American meteorological society* 78(2):197–208 1565
1566
1567
- Kim JE, Laguë MM, Pennypacker S, et al (2020) Evaporative Resistance is of Equal Importance as Surface Albedo in High-Latitude Surface Temperatures Due to Cloud Feedbacks. *Geophysical Research Letters* 47(4). <https://doi.org/10.1029/2019GL085663> 1568
1569
1570
1571
1572
- Kirshbaum DJ, Smith RB (2009) Orographic precipitation in the tropics: Large-Eddy simulations and theory. *Journal of the Atmospheric Sciences* 66(9):2559–2578. <https://doi.org/10.1175/2009JAS2990.1> 1573
1574
1575
1576
- Kirtman BP, Shukla J (2000) Influence of the Indian summer monsoon on ENSO. *Quarterly Journal of the Royal Meteorological Society* 126(562):213–239. <https://doi.org/10.1002/qj.49712656211> 1577
1578
1579
- Kite ES, Ford EB (2018) Habitability of Exoplanet Waterworlds. *The Astrophysical Journal* 864(1):75. <https://doi.org/10.3847/1538-4357/aad6e0> 1580
1581
1582
- Knippertz P, Wernli H (2010) A Lagrangian Climatology of Tropical Moisture Exports to the Northern Hemispheric Extratropics. *Journal of Climate* 23(4):987–1003. <https://doi.org/10.1175/2009JCLI3333.1> 1583
1584
1585
1586
- Kooperman GJ, Chen Y, Hoffman FM, et al (2017) Forest response to rising CO₂ drives zonally asymmetric rainfall change over tropical continents. *Nature Climate Change* 8(5):1–36. <https://doi.org/10.1038/s41558-018-0144-7> 1587
1588
1589
1590
1591
- Kottek M, Grieser J, Beck C, et al (2006) World map of the Köppen-Geiger climate classification updated. *Meteorologische Zeitschrift* 15(3):259–263. <https://doi.org/10.1127/0941-2948/2006/0130> 1592
1593
1594
1595
- Laguë MM, Bonan GB, Swann ALS (2019) Separating the Impact of Individual Land Surface Properties on the Terrestrial Surface Energy Budget in both the Coupled and Uncoupled Land–Atmosphere System. *Journal of Climate* 32(18):5725–5744. <https://doi.org/10.1175/jcli-d-18-0812.1> 1596
1597
1598
1599
1600
- Laguë MM, Pietschnig M, Ragen S, et al (2021) Terrestrial evaporation and global climate: Lessons from Northland, a planet with a hemispheric continent. *Journal of Climate* 34(6):2253–2276. <https://doi.org/10.1175/jcli-d-20-0452.1> 1601
1602
1603
1604
- Loft G (1918) The Gulf Stream and the North Atlantic Drift. *Journal of Geography* 17(1):8–17. <https://doi.org/10.1080/00221341808984367> 1605
1606
1607
- Macdonald FA, Swanson-hysell NL, Park Y, et al (2019) Arc-continent collisions in the tropics set Earth's climate state. *Science* 184(April):181–184 1608
1609
1610

- 1611 Manabe S, Terpstra TB (1974) The effect of mountains on the general
 1612 circulation of the Atmosphere. *Journal of the Atmospheric Sciences* 31(1):3
 1613
- 1614 Manabe SYUKURO (1969) Climate and the Ocean Circulation. *Monthly*
 1615 *Weather Review* 97(11):739–774. [https://doi.org/10.1175/1520-0493\(1969\)](https://doi.org/10.1175/1520-0493(1969)097(0739:CATOC)2.3.CO;2)
 1616 [097\(0739:CATOC\)2.3.CO;2](https://doi.org/10.1175/1520-0493(1969)097(0739:CATOC)2.3.CO;2)
- 1617
- 1618 Maroon EA, Frierson DM (2016) The impact of a continent’s longi-
 1619 tudinal extent on tropical precipitation. *Geophysical Research Letters*
 1620 43(22):11,921–11,929. <https://doi.org/10.1002/2016GL071518>
- 1621
- 1622 Maroon EA, Frierson DM, Battisti DS (2015) The tropical precipita-
 1623 tion response to Andes topography and ocean heat fluxes in an aqua-
 1624 planet model. *Journal of Climate* 28(1):381–398. [https://doi.org/10.1175/](https://doi.org/10.1175/JCLI-D-14-00188.1)
 1625 [JCLI-D-14-00188.1](https://doi.org/10.1175/JCLI-D-14-00188.1)
- 1626
- 1627 McFarlane NA (1987) The Effect of Orographically Excited Gravity Wave
 1628 Drag on the General Circulation of the Lower Stratosphere and Troposphere.
 1629 *Journal of the Atmospheric Sciences* 44(14):1775–1800. [https://doi.org/10.](https://doi.org/10.1175/1520-0469(1987)044<1775:teooeg>2.0.co;2)
 1630 [1175/1520-0469\(1987\)044<1775:teooeg>2.0.co;2](https://doi.org/10.1175/1520-0469(1987)044<1775:teooeg>2.0.co;2)
- 1631
- 1632 Méndez A, Rivera-Valentín EG, Schulze-Makuch D, et al (2021) Habitability
 1633 Models for Astrobiology. *Astrobiology* 21(8):1017–1027. [https://doi.org/10.](https://doi.org/10.1089/ast.2020.2342)
 1634 [1089/ast.2020.2342](https://doi.org/10.1089/ast.2020.2342)
- 1635
- 1636 Merdith AS, Williams SE, Collins AS, et al (2021) Extending full-plate
 1637 tectonic models into deep time: Linking the Neoproterozoic and the Phanero-
 1638 zoic. *Earth-Science Reviews* 214(December 2020):103,477. [https://doi.org/](https://doi.org/10.1016/j.earscirev.2020.103477)
 1639 [10.1016/j.earscirev.2020.103477](https://doi.org/10.1016/j.earscirev.2020.103477)
- 1640
- 1641 Mlawer EJ, Taubman SJ, Brown PD, et al (1997) Radiative transfer for inho-
 1642 mogeneous atmospheres: RRTM, a validated correlated-k model for the
 1643 longwave. *Journal of Geophysical Research: Atmospheres* 102(D14):16,663–
 1644 16,682. <https://doi.org/10.1029/97JD00237>
- 1645
- 1646 North GR, Mengel JG, Short DA (1983) Simple energy balance model resolving
 1647 the seasons and the continents: Application to the astronomical theory of
 1648 the ice ages. *Journal of Geophysical Research* 88(C11):6576–6586. <https://doi.org/10.1029/JC088iC11p06576>
- 1649
- 1650 Payne RE (1972) Albedo of the Sea Surface. *Journal of the Atmospheric*
 1651 *Sciences* 29(5):959–970. [https://doi.org/10.1175/1520-0469\(1972\)029<0959:](https://doi.org/10.1175/1520-0469(1972)029<0959:aotss>2.0.co;2)
 1652 [aotss>2.0.co;2](https://doi.org/10.1175/1520-0469(1972)029<0959:aotss>2.0.co;2)
- 1653
- 1654 Penn JL, Deutsch C, Payne JL, et al (2018) Temperature-dependent hypoxia
 1655 explains biogeography and severity of end-Permian marine mass extinction.
 1656 *Science* 362(6419). <https://doi.org/10.1126/science.aat1327>

- Pierrehumbert RT (2010) Principles of Planetary Climate, 1st edn. Cambridge University Press, <https://doi.org/10.1017/CBO9780511780783>
- Pietschnig M, Swann AL, Lambert FH, et al (2021) Response of tropical rainfall to reduced evapotranspiration depends on continental extent. *Journal of Climate* 34(23):9221–9234. <https://doi.org/10.1175/JCLI-D-21-0195.1>
- Queney P (1948) The Problem of Air Flow Over Mountains: A Summary of Theoretical Studies. *Bulletin of the American Meteorological Society* 29(1):16–26. <https://doi.org/10.1175/1520-0477-29.1.16>
- Richardson PL (1980) Benjamin Franklin and Timothy Folger’s First Printed Chart of the Gulf Stream. *Science* 207(4431):643–645
- Rushby AJ, Shields AL, Wolf ET, et al (2020) The Effect of Land Albedo on the Climate of Land-dominated Planets in the TRAPPIST-1 System. *The Astrophysical Journal* 904(2):124. <https://doi.org/10.3847/1538-4357/abbe04>
- Salem BBC (1989) Arid zone forestry: A guide for field technicians. FAO Conservation Guide No. 20
- Saulière J, Brayshaw DJ, Hoskins B, et al (2012) Further Investigation of the Impact of Idealized Continents and SST Distributions on the Northern Hemisphere Storm Tracks. *Journal of the Atmospheric Sciences* 69(3):840–856. <https://doi.org/10.1175/JAS-D-11-0113.1>
- Seager S (2013) Exoplanet Habitability. *The Astrophysical Journal* 340(May):577–582. <https://doi.org/10.1088/0004-637X/777/2/95>
- Shukla J, Mintz Y (1982) Influence of Land-Surface Evapotranspiration on the Earth’s Climate. *Science* 215(4539):1498–1501. <https://doi.org/10.1126/science.215.4539.1498>
- Sikma M, Vilà-Guerau de Arellano J (2019) Substantial Reductions in Cloud Cover and Moisture Transport by Dynamic Plant Responses. *Geophysical Research Letters* 46(3):1870–1878. <https://doi.org/10.1029/2018GL081236>
- Stefan J (1879) On the relationship between thermal radiation and temperature. *Bulletin from the sessions of the Vienna Academy of Sciences (Vienna, 1879)* 79:391–428
- Stone PH (1978) Baroclinic Adjustment. *Journal of the Atmospheric Sciences* 35(April):561–571
- Straume EO, Gaina C, Medvedev S, et al (2020) Global Cenozoic Paleobathymetry with a focus on the Northern Hemisphere Oceanic Gateways.

- 1703 Gondwana Research 86:126–143. <https://doi.org/10.1016/j.gr.2020.05.011>
1704
- 1705 Sud YC, Shukla J, Mintz Y (1988) Influence of Land Surface Roughness on
1706 Atmospheric Circulation and Precipitation: A Sensitivity Study with a Gen-
1707 eral Circulation Model. *Journal of Applied Meteorology* 27(9):1036–1054.
1708 [https://doi.org/10.1175/1520-0450\(1988\)027<1036:iolsro>2.0.co;2](https://doi.org/10.1175/1520-0450(1988)027<1036:iolsro>2.0.co;2)
1709
- 1710 Thomson SI, Vallis GK (2019) Hierarchical modeling of solar sys-
1711 tem planets with Isca. *Atmosphere* 10(12):1–21. [https://doi.org/10.3390/](https://doi.org/10.3390/ATMOS10120803)
1712 [ATMOS10120803](https://doi.org/10.3390/ATMOS10120803)
- 1713 Tierney JE, Poulsen CJ, Montañez IP, et al (2020) Past climates inform
1714 our future. *Science* 370(6517):eaay3701. [https://doi.org/10.1126/science.](https://doi.org/10.1126/science.aay3701)
1715 [aay3701](https://doi.org/10.1126/science.aay3701)
1716
- 1717 Vallis GK, Colyer G, Geen R, et al (2018) Isca, v1.0: A framework for the
1718 global modelling of the atmospheres of Earth and other planets at varying
1719 levels of complexity. *Geoscientific Model Development* 11(3):843–859. <https://doi.org/10.5194/gmd-11-843-2018>
1720
1721
- 1722 Van Rossum G, Drake FL (2009) *Python 3 Reference Manual*. CreateSpace,
1723 Scotts Valley, CA, <https://doi.org/10.5555/1593511>
1724
- 1725 Virtanen P, Gommers R, Oliphant TE, et al (2020) SciPy 1.0: Fundamental
1726 algorithms for scientific computing in Python. *Nature Methods* 17(3):261–
1727 272. <https://doi.org/10.1038/s41592-019-0686-2>
1728
- 1729 Voigt A (2013) The dynamics of the Snowball Earth Hadley circulation for
1730 off-equatorial and seasonally varying insolation. *Earth System Dynamics*
1731 4(2):425–438. <https://doi.org/10.5194/esd-4-425-2013>
1732
- 1733 Voigt A, Held IM, Marotzke J (2012) Hadley cell dynamics in a virtually dry
1734 snowball Earth atmosphere. *Journal of the Atmospheric Sciences* 69(1):116–
1735 128. <https://doi.org/10.1175/JAS-D-11-083.1>
- 1736 Voigt A, Bony S, Dufresne JL, et al (2014) The radiative impact of clouds
1737 on the shift of the Intertropical Convergence Zone. *Geophysical Research*
1738 *Letters* 41(12):4308–4315. <https://doi.org/10.1002/2014GL060354>
1739
- 1740 Voosen P (2019) A 500-million-year survey of Earth’s climate reveals dire
1741 warning for humanity. *Science* <https://doi.org/10.1126/science.aay1323>
1742
- 1743 White RH, Battisti DS, Roe GH (2017) Mongolian mountains matter most:
1744 Impacts of the latitude and height of asian orography on pacific wintertime
1745 atmospheric circulation. *Journal of Climate* 30(11):4065–4082. [https://doi.](https://doi.org/10.1175/JCLI-D-16-0401.1)
1746 [org/10.1175/JCLI-D-16-0401.1](https://doi.org/10.1175/JCLI-D-16-0401.1)
1747
1748

Wiscombe W, Warren S (1980) A Model for Spectral Albedo I: Pure Snow	1749
	1750
Worsley TR, Kidder DL (1991) First-order coupling of paleogeography and CO ₂ , with global surface temperature and its latitudinal contrast. <i>Geology</i> 19(12):1161–1164. <a href="https://doi.org/10.1130/0091-7613(1991)019<1161:FOCOPA>2.3.CO;2">https://doi.org/10.1130/0091-7613(1991)019<1161:FOCOPA>2.3.CO;2	1751
	1752
	1753
	1754
	1755
Yasunari T, Saito K, Takata K (2006) Relative roles of large-scale orography and land surface processes in the global hydroclimate. Part I: Impacts on monsoon systems and the tropics. <i>Journal of Hydrometeorology</i> 7(4):626–641. https://doi.org/10.1175/JHM515.1	1756
	1757
	1758
	1759
	1760
Zelinka MD, Randall DA, Webb MJ, et al (2017) Clearing clouds of uncertainty. <i>Nature Climate Change</i> 7(10):674–678. https://doi.org/10.1038/nclimate3402	1761
	1762
	1763
	1764
Zhai J, Boos WR (2017) The drying tendency of shallow meridional circulations in monsoons. <i>Quarterly Journal of the Royal Meteorological Society</i> 143(708):2655–2664. https://doi.org/10.1002/qj.3091	1765
	1766
	1767
	1768
Zhou W, Xie SP (2018) A hierarchy of idealized monsoons in an intermediate GCM. <i>Journal of Climate</i> 31(22):9021–9036. https://doi.org/10.1175/JCLI-D-18-0084.1	1769
	1770
	1771
	1772
	1773
	1774
	1775
	1776
	1777
	1778
	1779
	1780
	1781
	1782
	1783
	1784
	1785
	1786
	1787
	1788
	1789
	1790
	1791
	1792
	1793
	1794